NASA TECHNICAL NOTE

NASA TN D-6111

DEVELOPMENT OF A SIMULATOR FOR STUDYING SIMPLIFIED LUNAR ESCAPE SYSTEMS

by George J. Hurt, Jr., David B. Middleton, and Marion A. Wise

Langley Research Center
Hampton, Va. 23365

NATIONAL AERONAUTICS AND SPACE ADMINISTRATION • WASHINGTON, D. C. • APRIL 1971

1. Report No.	2. Government Accession No.	3.
NASA TN D-6111		

4. Title and Subtitle	5. Report Date
DEVELOPMENT OF A SIMULATOR FOR STUDYING SIMPLIFIED LUNAR ESCAPE SYSTEMS	April 1971
	6. Performing Organization Code
7. Author(s) George J. Hurt, Jr., David B. Middleton, and Marion A. Wise	8. Performing Organization Report No. L-7364
	10. Work Unit No. 127-51-41-04
9. Performing Organization Name and Address NASA Langley Research Center Hampton, Va. 23365	11. Contract or Grant No.
	13. Type of Report and Period Covered Technical Note
12. Sponsoring Agency Name and Address National Aeronautics and Space Administration Washington, D.C. 20546	14. Sponsoring Agency Code

15. Supplementary Notes

16. Abstract

A lunar-escape-system simulator was designed and fabricated to be used as a research tool to study problems related to lunar escape and simplified manual guidance and control. The design involved a two-man platform with instruments and controllers mounted on a strain-gage base. Most of the vehicle characteristics and control logic were contained in the computer program; thus a wide range of vehicles (including the lunar flying vehicles) and guidance and control systems could be studied. The computer program was compared with an independent computer program with good agreement. During checkout operations the subjects were able to adapt to the equipment with a minimum of training and instruction in the operation of the simulator.

17. Key Words (Suggested by Author(s))	18. Distribution Statement
Guidance Instrumentation Lunar escape Flying platforms	Unclassified – Unlimited

19. Security Classif. (of this report)	20. Security Classif. (of this page)	21. No. of Pages	22. Price*
Unclassified	Unclassified	45	$3.00

*For sale by the National Technical Information Service, Springfield, Virginia 22151

DEVELOPMENT OF A SIMULATOR FOR STUDYING SIMPLIFIED LUNAR ESCAPE SYSTEMS

By George J. Hurt, Jr., David B. Middleton,
and Marion A. Wise
Langley Research Center

SUMMARY

A lunar-escape-system simulator was designed and fabricated to be used as a research tool to study problems related to lunar escape and simplified manual guidance and control. The primary requirements for the simulator were based on items that would be desirable for an actual lunar escape system: first, simplified propulsion; second, a simplified stabilization and control method; and third, a simplified guidance and navigation technique. To ensure exact trajectory calculations the real-time digital computer program used in the simulation was compared with an independent computer program, and good agreement was obtained.

The facility design included load cells to transmit pilot kinesthetic control motions realistically. Most of the vehicle characteristics and control logic were contained in the computer program; thus investigation of a wide range of vehicles (including the lunar flying vehicles) and guidance and control systems was possible. During checkout operations test subjects were able to adapt to the equipment with a minimum of training and instruction in the operation of the simulator.

INTRODUCTION

The ascent stage of the lunar module (LM) includes many redundancies and other features to maximize its chance of successful operation. It must, however, rely on a single rocket engine for lift-off; an alternate means of escaping to lunar orbit is thus highly desirable. A number of approaches have been suggested including multipurpose surface-to-orbit shuttlecraft and lunar flying vehicles (LFV) with the capability of also achieving lunar orbit. Both of these approaches involve rather extensive development time and probably a separate earth launch to place the vehicles on the moon.

A third approach which has for several years been considered at NASA Langley Research Center (LRC) is that of packaging a very simplified lunar escape system (LES)

on the LM (see refs. 1 to 4). Primary emphasis has been on the development of appropriate guidance and control techniques and determination of stability requirements for a simplified LES. Some effort at LRC has also been directed toward development of a dual-purpose LFV-LES. The problem of unloading, setting up, and servicing an LES (or LFV) on the moon is also discussed in these references.

Flight-simulation studies are now essential in determining the feasibility of using particular minimum-complexity LES configurations, control modes, and guidance techniques. A lunar-escape-system simulator (LESS) has been developed at LRC to study such problems. Throughout this report the lunar escape system will be referred to as the LES; the simulator of that system will be LESS. The primary requirements for the LESS were based on items that would be desirable for an actual lunar escape system: first, simplified propulsion; second, a simplified stabilization and control method; and third, a simplified guidance and navigation technique.

The LESS is the subject of the present report, which covers the development of simulation hardware and an associated real-time digital computer program. Most of the vehicle characteristics and control logic are contained in the computer program; thus investigation of a wide range of vehicles (including the LFV) and guidance and control systems is possible. The real-time computer program has been compared with an independent digital computer program with good agreement. The LESS is operational at present and has proved to be a useful representation of the pilot problems involved in using either jets or kinesthetic inputs for attitude control.

SYMBOLS

Values are given in both SI and U.S. Customary Units. The measurements and calculations were made in U.S. Customary Units.

A_e cross-sectional area of exit nozzle of rocket main thruster

a semimajor axis of vehicle orbit

a_{ij} direction-cosine elements of matrix used for transformation from body to inertial system (i=1,2,3; j=1,2,3)

b_{ij} direction-cosine elements of matrix used for transformation from body to local-vertical system (i=1,2,3; j=1,2,3)

c_{ij} direction-cosine elements of matrix used for transformation from inertial to local-vertical system (i=1,2,3; j=1,2,3)

D_1, D_2, D_3 auxiliary variables used to simplify moment equations in appendix B

F magnitude of $\overline{F}$ (or gage thrust)

F_1, F_2 maximum and intermediate constant magnitudes of $\overline{F}$

F_h magnitude of $\overline{F}_h$

$F_{x_B}, F_{y_B}, F_{z_B}$ body-axis components of $\overline{F}$

$F^*_{x_B}, F^*_{y_B}, F^*_{z_B}$ body-axis components of $\overline{F}^*$

$\overline{F}$ force due to rocket engine (or to main thruster of LES, in particular)

$\overline{F}_{ext}$ external force acting on rocket mass

$\overline{F}_h$ horizontal restraining force of rocket test stand

$\overline{F}_R$ total restraining force of rocket test stand

$\overline{F}^*$ force due to combination of thrust and gravity

G vehicle reference point (viz., initial location of vehicle center of gravity (c.g.))

g_e acceleration due to earth gravity, 9.81 m/sec^2 (32.2 ft/sec^2)

g_m acceleration due to lunar gravity, 1.62 m/sec^2 (5.32 ft/sec^2)

h_a, h_p altitude of apocynthion and pericynthion, respectively

I_{sp} specific impulse of LES propellant mixture

I_{xx}, I_{yy}, I_{zz} moments of inertia of vehicle with respect to body axes

I_{xy}, I_{xz}, I_{yz} products of inertia of vehicle with respect to body axes

$I'_{xx_j}, I'_{yy_j}, I'_{zz_j}$ moments of inertia of m_j with respect to temporary axes X, Y, and Z through the c.g.'s of m_j (j=1,2,...,5)

I'_{xz_j} products of inertia of m_j with respect to temporary axes X and Z through the c.g.'s of m_j (j=1,2,...,5)

$(dI_{xx})_{disk}, (dI_{zz})_{disk}$ differential moment of inertia of elemental propellant disk with respect to temporary axes X and Z through center of the disk

m instantaneous mass of vehicle

m_i elemental mass particles which comprise m (i=1,2,...,∞)

m_j mass modules which comprise m (j=1,2,...,5)

$m_{5,o}$ initial propellant mass

$\bar{N}_O$ angular momentum of vehicle about its instantaneous c.g. (point O)

$N_{x_B}, N_{y_B}, N_{z_B}$ body-axis components of $\bar{N}_O$

O location of instantaneous c.g. of vehicle (also origin of body axes X_B, Y_B, and Z_B)

p_e magnitude of $\bar{p}_e$

$\bar{p}_e$ directional rocket-exhaust pressure at nozzle exit

p,q,r components of angular velocity measured about body axes X_B, Y_B, and Z_B, respectively

$Q_{J,x_B}, Q_{J,y_B}, Q_{J,z_B}$ body-axis torques due to attitude jets

Q_{P,x_B}, Q_{P,y_B} miscellaneous body-axis torques

$Q_{x_B}, Q_{y_B}, Q_{z_B}$ body-axis components of total body torque

$\bar{R}_G, \bar{R}_O$ position vectors of point G and point O with respect to center of moon

$\bar{R}_i$ position vectors of m_i with respect to center of moon (i=1,2,...,∞)

R_O magnitude of $\bar{R}_O$

$R_{x_B}, R_{y_B}, R_{z_B}$ body-axis components of $\bar{R}_O$

$R_{x_I}, R_{y_I}, R_{z_I}$ inertial components of $\bar{R}_O$

$\bar{r}_{GO}$ position vector of point O with respect to point G

$\bar{r}_i$ position vectors of m_i with respect to point G ($i=1,2,\ldots,\infty$)

r_m radius of moon

r_p radius of pericynthion

r_s radius of spherical propellant tank

t time

t_1, t_2, t_3 time of beginning, midpoint, and end, respectively, of the 90^o LES pitch-transition maneuver (pitchover)

t_{BO} time of burnout

u, v, w body-axis components of $\bar{v}_O$

u', v', w' body-axis components of $\bar{v}_G$

dV elemental volume of disk of propellant

V_{z_B} simulated velocity-along-the-thrust-axis signal

v_e magnitude of $\bar{v}_e$

$v_{O,h}$ horizontal component of $\bar{v}_O$

$\bar{v}$ velocity of general rocket mass used in derivation of force equations

$\bar{v}_e$ effective exhaust velocity of rocket-engine gas particles with respect to m

$\bar{v}_G$ total linear velocity of point G with respect to center of moon

$\bar{v}_O$ total linear velocity of point O with respect to center of moon

$\bar{v}_{GO}$ velocity of point O with respect to point G

x,y,z distances (or directions) in X,Y,Z system

x_B,y_B,z_B distances (or directions) in X_B,Y_B,Z_B system

$x_{G,j},y_{G,j},z_{G,j}$ body-axis components of initial positions of $\bar{\rho}_{m_j}$ $(j=1,2,\ldots,5)$

x_I,y_I,z_I distances in X_I,Y_I,Z_I system

x_i,y_i,z_i body-axis components of $\bar{r}_i$ $(i=1,2,\ldots,\infty)$

x_{LV},y_{LV},z_{LV} distances in X_{LV},Y_{LV},Z_{LV} system

$z_{B,t}$ displacement distance of thruster gimbal below point G (measured along Z_B-axis)

z_1 distance from center of propellant tank to propellant surface

β out-of-plane angle

$\Delta x,\Delta y,\Delta z$ body-axis components of $\bar{r}_{GO}$

$\delta_{x_B,3},\delta_{y_B,3}$ body-axis components of control pilot's c.g. shift

$\delta_{z_B,5}$ c.g. shift of propellant mass with respect to center of spherical tank

η down-range angle

φ,ψ,θ Euler angles used in transformation from body to inertial system

φ',ψ',θ' Euler angles used in transformation from body to local-vertical system

θ_1,θ_2 constant pitch angles used before and after pitchover, respectively

μ lunar gravitational constant, 4.9028×10^{12} m^3/sec^2 (1.7314×10^{14} ft^3/sec^2)

ξ_{x_B}, ξ_{y_B} body-axis components of the thrust-misalinement angle

$\bar{\rho}_{m_j}$ position vectors from the vehicle instantaneous c.g. to the component masses m_j (j=1,2,...,5)

$\rho_{x_j}, \rho_{y_j}, \rho_{z_j}$ body-axis components of $\bar{\rho}_{m_j}$ (j=1,2,...,5)

σ propellant mass density

$\omega_{B,x_I}, \omega_{B,y_I}, \omega_{B,z_I}$ inertial-axis components of body-axis rotational rate

$\omega_{LV,x_I}, \omega_{LV,y_I}, \omega_{LV,z_I}$ inertial-axis components of rotational rate of the local vertical

$\omega_{x_{LV}}, \omega_{y_{LV}}, \omega_{z_{LV}}$ components of $\bar{\omega}$ measured in local-vertical axis system

$\bar{\omega}$ total rotational rate of vehicle about point O

Axis systems (all systems initially parallel):

X_B, Y_B, Z_B body axes with origin at instantaneous c.g. of vehicle (point O)

X_G, Y_G, Z_G initial location of X_B, Y_B, Z_B (point O ≡ point G)

X_I, Y_I, Z_I inertial axes (Z_I lies along local vertical at lift-off site, and the $X_I Z_I$-plane coincides with plane of command-service-module orbit)

X_{LV}, Y_{LV}, Z_{LV} local-vertical axes with origin at point O (Z_{LV} is parallel to local vertical, and Y_{LV} is parallel to Y_I)

X,Y,Z temporary axes with origin placed in convenient locations to aid in intermediate calculations (such as moments of inertia of m_j (j=1,2,...,5) with respect to c.g. of each m_j)

A dot over a variable denotes differentiation with respect to time. A matrix inverse is denoted by $[\ ]^{-1}$, and body-axis components of a vector are denoted by $[,,]$.

DESIGN CONSIDERATIONS

In a real emergency lunar escape situation, it seems reasonable (see ref. 5) to require the astronauts to perform a number of guidance and control functions which would normally be handled automatically by LM onboard systems. This approach would lead to minimum-complexity hardware, which allows (1) possible stowage of the LES on the LM, (2) a relatively shorter LES development time, and (3) the high reliability associated with simplified systems. In particular, it seems desirable to limit the dry mass of the LES to approximately 135 kg (300 lbm); this limitation suggests that use must be made of the LM propellants (which become available in an emergency escape situation). The minimum weight of a suitable hypergolic propulsion system (engine, tanks, pressurization system, etc.) could exceed one-half of this dry-mass allotment; this requirement dictates a very simple and lightweight LES vehicle structure with very little instrumentation.

Mission Requirements

The basic mission requirements postulated for an emergency escape situation are the following:

(1) The LES must lift two astronauts from the lunar surface to a safe lunar orbit. (By definition a safe lunar orbit must have a pericynthion altitude greater than 15 240 meters (50 000 feet).)

(2) The orbiting command service module (CSM) must rendezvous with the LES and pick up the two LES astronauts within the 4-hour operating limit of their portable life support systems (PLSS). Another constraint is that the CSM must make the rendezvous within its energy allocation for LM rescue (at present, this allocation corresponds to a CSM characteristic velocity of approximately 240 m/sec (787 ft/sec).

In addition to the basic mission requirements, the following assumptions are made for the LESS study:

(1) The LES must be capable of being controlled by one astronaut. The second astronaut will be strictly control-inactive, although he may have some monitoring or communications duties.

(2) On the lunar surface the LES will have c.g. sensing capability (e.g., load cells), which will allow the LES pilot to adjust the c.g. onto the expected thrust line for lift-off.

(3) The required time of lift-off is known, either from communication with or visual sighting of the CSM.

(4) Four propellant tanks are symmetrically arrayed with no propellant slosh (i.e., by use of positive expulsion bladders).

(5) The astronauts will use the LM life support provisions until just prior to LES lift-off. After lift-off the astronaut's PLSS will be necessary in the open cockpit of the LES.

An artist's concept of a LES is shown in figure 1.

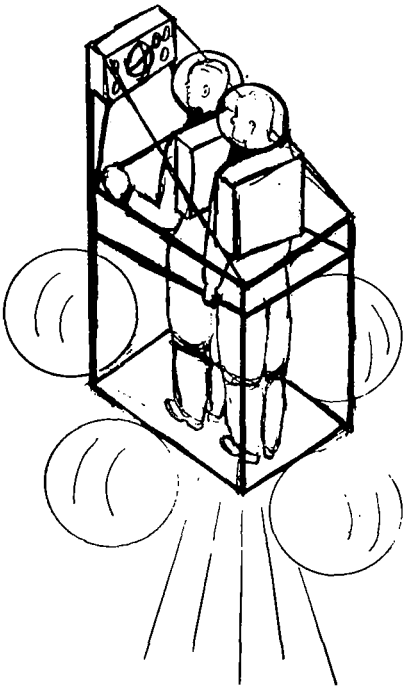

Figure 1.- An artist's concept of a LES.

Guidance Considerations

Guidance requirements of the LES are relaxed somewhat by the assumption that the CSM will perform the rendezvous. For this reason and also because of LES weight limitations, only unsophisticated guidance techniques are considered in the LESS studies. For example, holding the LES vehicle attitude to a series of constant pitch angles for specified time intervals is an open-loop method of launching into orbit, which requires only a clock and simple attitude indicators for instrumentation. An improved variation may be a three-axis attitude indicator (8-ball) and the digital readout of an integrating accelerometer to provide velocity information.

Control Techniques

Several attitude control techniques requiring little or no control mechanization are being considered in the LESS studies. One is kinesthetic (balance-reflex) control of pitch and roll, which reduces attitude controller requirements from a three-axis hand controller

to a three-position on-off yaw switch (or stick). The type of kinesthetic control considered for the LESS studies involves the ability of the control pilot to change and/or correct his attitudes by shifting his c.g. with respect to the vehicle line of thrust. From a standing position he can lean (or step) forward to shift his body c.g. (and consequently the total-system c.g.) forward of the thrust line and thereby induce a pitch-down vehicle torque. Similar torques are induced about the roll axis by leaning sideways (see fig. 2).

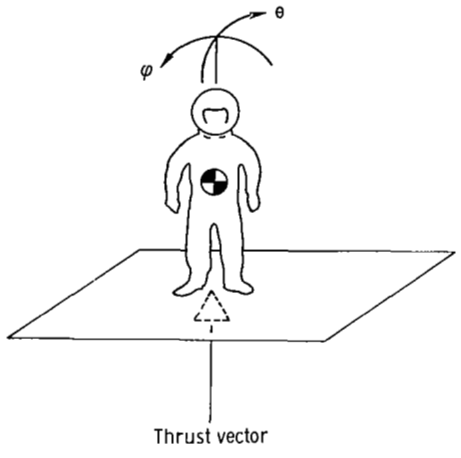

Figure 2.- The kinesthetic motion used by a pilot to initiate pitch and roll moments with respect to the vehicle line of thrust.

Kinesthetic control in various forms has been studied for a number of years (refs. 6 to 8) and found to be possible but not desirable for most flight applications requiring precise control, particularly during landing. Lunar escape requires no landings; thus kinesthetic control may be feasible. In addition, it appears that kinesthetic control should require very little training because it makes use of the pilot's inherent ability to keep his balance.

A second attitude control technique, thrust-vector control, requires very simple mechanization. A single main thruster can be double-gimbaled, and direct mechanical linkages between this thruster and a hand controller allow the pilot to tilt the thruster to generate pitch and roll moments. Jetavators or appropriate flaps on the thruster nozzle can be similarly linked to the controller for yaw control. With thrust-vector control, the pilot can either stand or be seated; if seated, he is less likely to introduce disturbing torques through inadvertent body shifts while operating the controllers. In some instances the pilot may wish to shift the total system c.g. intentionally in order to compensate for a bias torque (e.g., a torque due to thrust misalinement). If standing, he can step in the appropriate direction; if seated, he can reposition his legs.

The LESS is also appropriate for the study of other control techniques, such as using attitude jets only, or any combination of the techniques just mentioned.

LUNAR-ESCAPE-SYSTEM SIMULATOR

General Description of LESS Hardware and Computer Program

A lunar-escape-system simulator (LESS) was designed and fabricated to be used as a research tool to study problems related to lunar escape. The LESS was designed to accommodate a broad spectrum of studies related to lunar escape and simplified manual control. The primary requirements for the LESS were based on items that would be desirable for an actual lunar escape system: first, simplified propulsion; second, a simplified stabilization and control method; and third, a simplified guidance and navigation technique. The basic simulator hardware consists of a fixed-base pilot control station appropriately tied into a digital computer which operates in real time. The fixed-base pilot control station includes provisions for (1) simplified thrust and attitude control, (2) instrument displays, and (3) equipment to sense the motions of a pilot's center of gravity (viz., strain-gage load cells). Features which can be added for particular studies are visual displays to the control pilot and free but limited pitch and roll motions of the control station itself.

Figure 3 is a block diagram showing the man-hardware-software relationships of the LESS. This diagram illustrates that the LESS pilot control station can accommodate two men (standing or seated) but that it is outfitted primarily for one-man control. Control inputs from the load cells and from the pilot's hand controllers are sent over telephone lines to the central computing complex where they enter the real-time computer through analog-to-digital signal converters. In turn, the computer updates the escape trajectory, calculates the instantaneous attitude of the vehicle with respect to a selected reference (e.g., the local vertical), and by means of digital-to-analog converters, returns selected analog signals to the simulator hardware. Several papers describing LRC simulation facilities are summarized in reference 9. One of these papers with direct

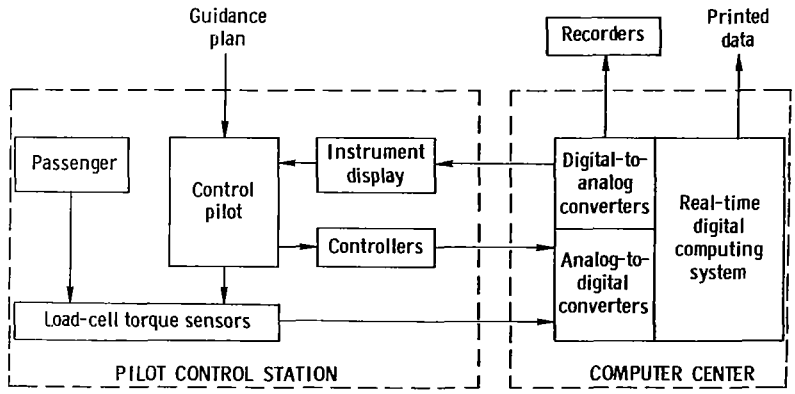

Figure 3.- Block diagram of lunar escape system simulator (LESS).

application to the LESS is entitled "A Description of LRC Digital Computer Complex and Special Features for Real-Time Simulation Applications." The LESS was set up to operate in the "multiprograming mode" described in this paper, and it "time-shared" with two other real-time simulations. A unique feature of the LESS system is some special circuitry and program logic which allows the pilot (at the remotely located pilot control station) to synchronize system operations by means of his thruster switch. For example, the computer can be used to calculate vehicle attitudes prior to lunar lift-off while the pilot is kinesthetically balancing the vehicle c.g. onto the expected line of thrust. Then, when thrust is turned on, the trajectory calculations begin and a discrete output signal from the computer starts the pilot's digital clock.

More detailed discussions of the simulator hardware and computer program are given in the sections which follow.

Pilot Control Station

A simulated pilot control platform was clamped to the top of a sandwich-type load-cell structure. The relative size of the simulator assembly is illustrated in figure 4, which shows the pilot and passenger in position for a simulated lift-off. The control-platform equipment included a handrail, a yaw attitude controller, a main-engine thrust controller, and a situation display panel.

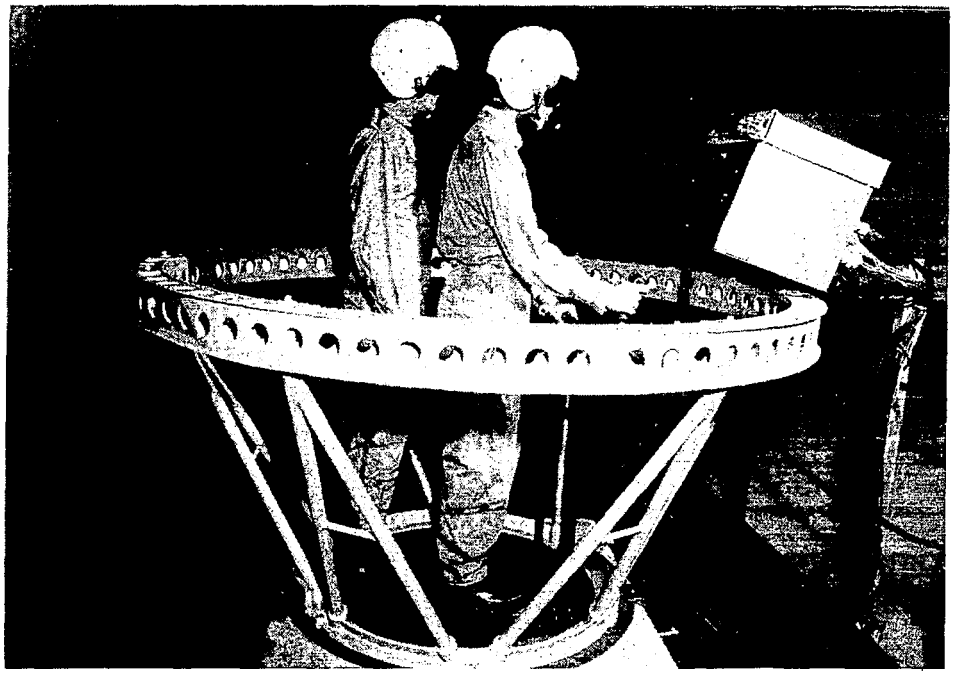

L-69-4990

Figure 4.- The simulator pilot-control station.

Figure 5 depicts the seated situation as provided for in the LESS design. A four-legged stool with a large footboard was placed on the LESS platform approximately over its c.g. For unbalanced pitching torques, the pilot can slide both feet forward or aft; for bias roll torques, he can shift one or both legs to one side.

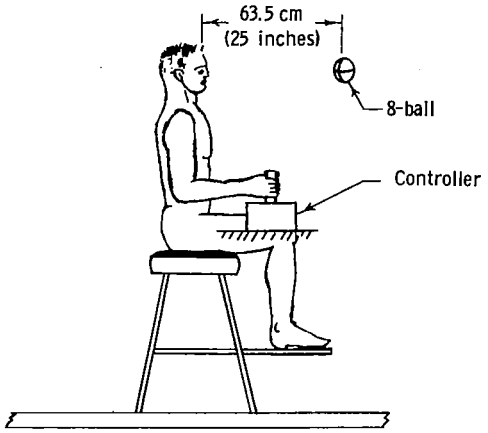

Figure 5.- Sketch of pilot in seated position.

Moment sensing.- A system of strain-gage load cells was used to sense the kinesthetic moments created by the pilot. The assembled load-cell sandwich and the amplifier rack are shown in figure 6. The orientation of the load cells is shown in figure 7. The main support post in the center of the platform acted as an $X_B Y_B$-logic pivot and was designed to carry the static weight of the simulator assembly. The main support post

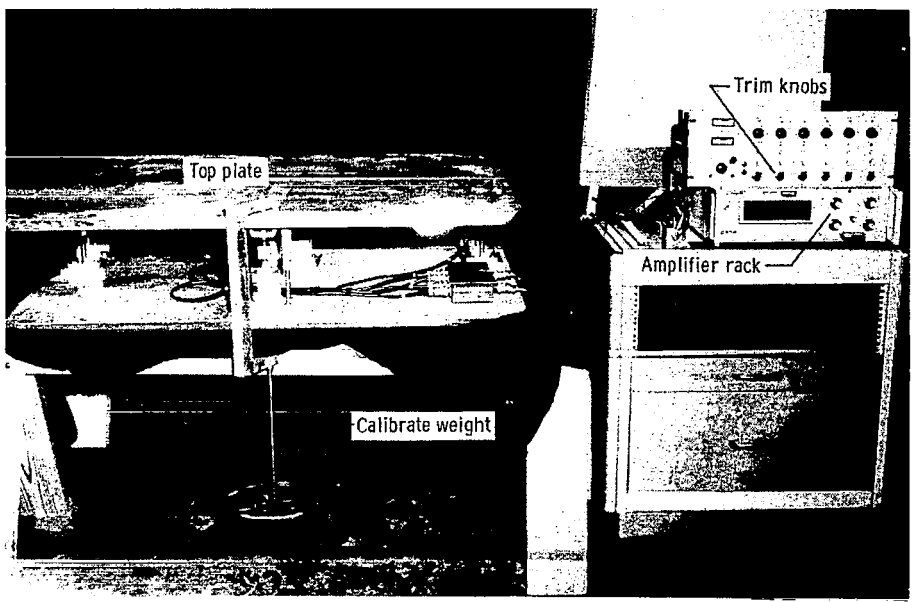

L-69-1570.1

Figure 6.- The assembled load-cell sandwich and the amplifier rack.

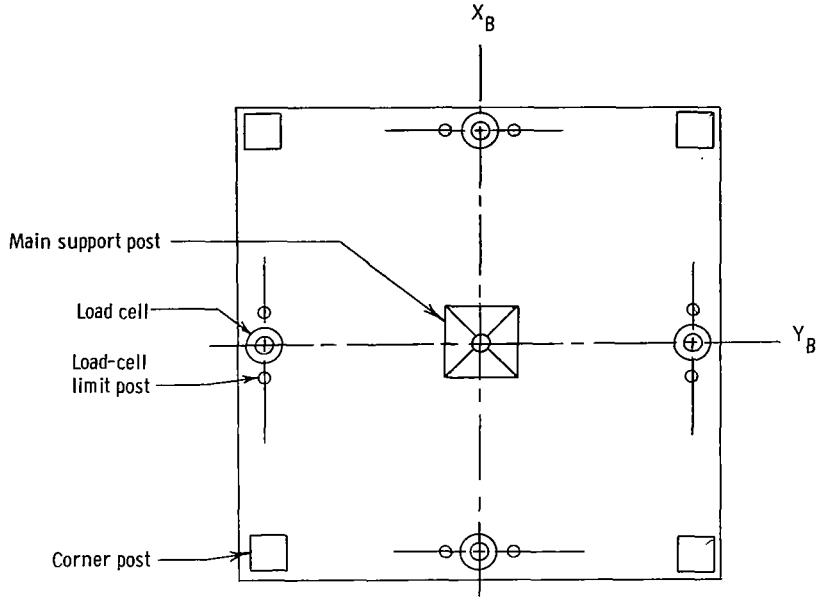

Figure 7.- A sketch of the load-cell orientation and associated hardware.

incorporated a flexure section designed to permit sufficient hinging of the upper plate to allow maximum rated deflection of the load cells. Each of the load-cell connector links to the upper plate also included a flexure post to isolate the load cells from shear loads that might be generated by pitch and roll moment combinations imposed on the upper plate. A mechanical deflection stop on each load cell and a caging mechanism consisting of four corner posts and wedges were used to avoid inadvertent overloads during simulator alterations and shutdown periods. Large offcenter loads, such as a passenger or display packages, were counterbalanced with lead weights. Minor day-to-day out-of-balance moments were trimmed to zero via a trim adjustment in the load-cell amplifier system.

Extraneous pickup from local 400-Hz and 60-Hz power lines was attenuated by filtering before transmission of the load-cell signals to the digital computer. This filtering also attenuated high-frequency components due to mechanical vibrations (the simulator was not mechanically isolated from the building).

Thrust and attitude controllers.- The three-position LESS thrust control switch is shown in figure 8. The full-down switch position is thrust off; the center position and full-up position are wired to command various levels of intermediate and maximum thrust, respectively.

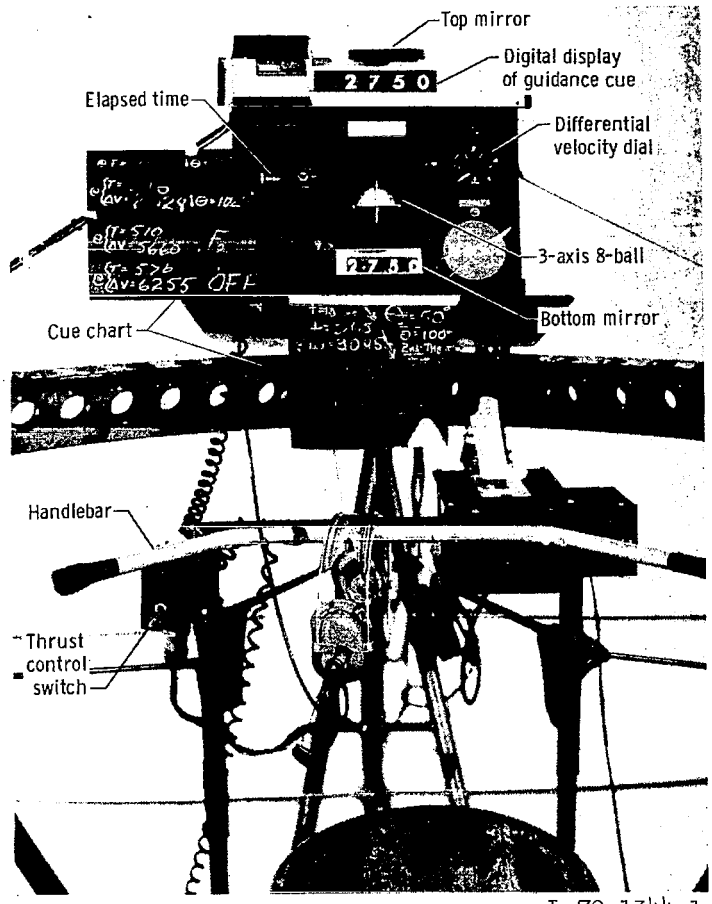

Figure 8.- The simulator control platform.

Two attitude controllers are provided at the pilot control station – a three-axis hand controller and a single-axis yaw stick controller. These controllers may be seen in figure 9. The three-axis controller shown is a CSM type (ref. 10). It is appropriate for most escape profiles in which attitude control is by thrust vectoring (gimbaled main engine) or in which there is all-jet attitude control. The yaw-output-signal conditioning was managed in the computer program. For the three-axis controller the attitude signals could be simple on-off pulses or proportional to controller deflections. An electrical dead band was used in each of the three controller axes to ensure a zero electrical signal output for each mechanical control center. When vehicle pitch and roll moments were to be controlled kinesthetically, the pitch and roll potentiometer outputs of the three-axis controller were grounded to prevent spurious control signals from being introduced into the computer program.

The single-axis yaw controller is a simple left-right spring-centered lever with microswitch contacts for signal initiation. The lever displacement required to generate a yaw input was fixed at a minimum.

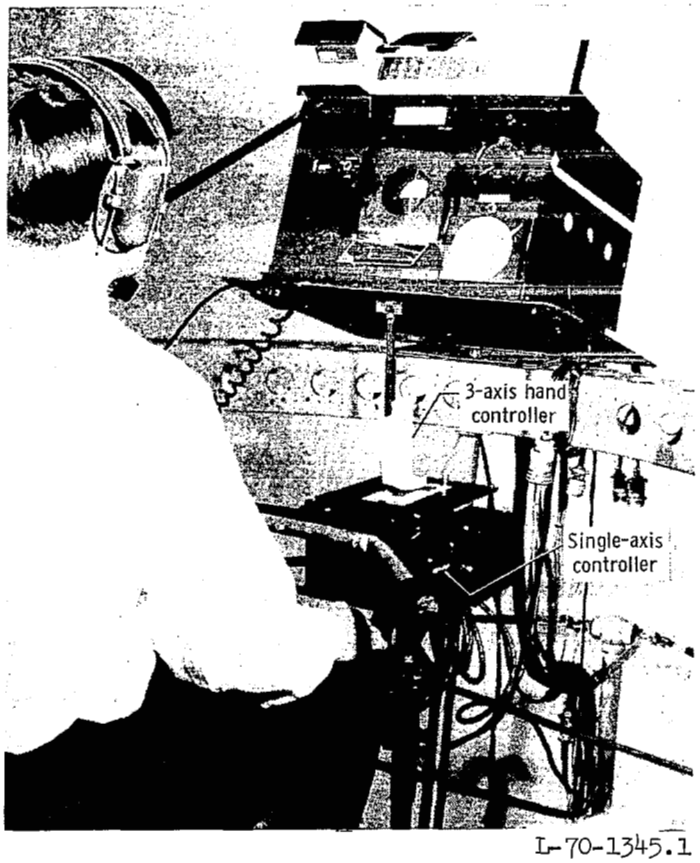

Figure 9.- The three-axis hand controller and the single-axis yaw controller.

Information displays.- In line with the simplified guidance and navigation concept, it was believed desirable to make some determination of the minimum attitude information necessary to enable the pilot to make a successful flight. The first information display group consisted of a digital clock, a fuel indicator, and a three-axis 8-ball. The instrument panel was hinged in order to accommodate the various eye-level heights which would be encountered (for the shortest subject seated to the tallest subject standing).

Vehicle attitude information was presented to the pilot by a three-axis 8-ball. The instrument used was a prototype instrument from a lunar-module attitude information group (see ref. 10). A full-face presentation of the 8-ball is shown in figure 10. Various functions of the 8-ball assembly were either masked off or altered to suit the LESS study requirement. The roll steering needle was programed to present out-of-plane information to the pilot during the trajectory. A displacement of the needle indicated the direction and relative magnitude of the out-of-plane velocity along the Y_B-axis. The pitch and yaw steering needles were not used for their normal function. They were coupled to the pitch and roll load-cell signals and used as vehicle leveling indicators for pitch and roll attitude during the prelaunch phase. The pitch and yaw needles were not used after

lift-off. Each of the three needles is shown in a displaced position in figure 10. A view of the instruments with the attitude rate information masked off is shown in figure 11.

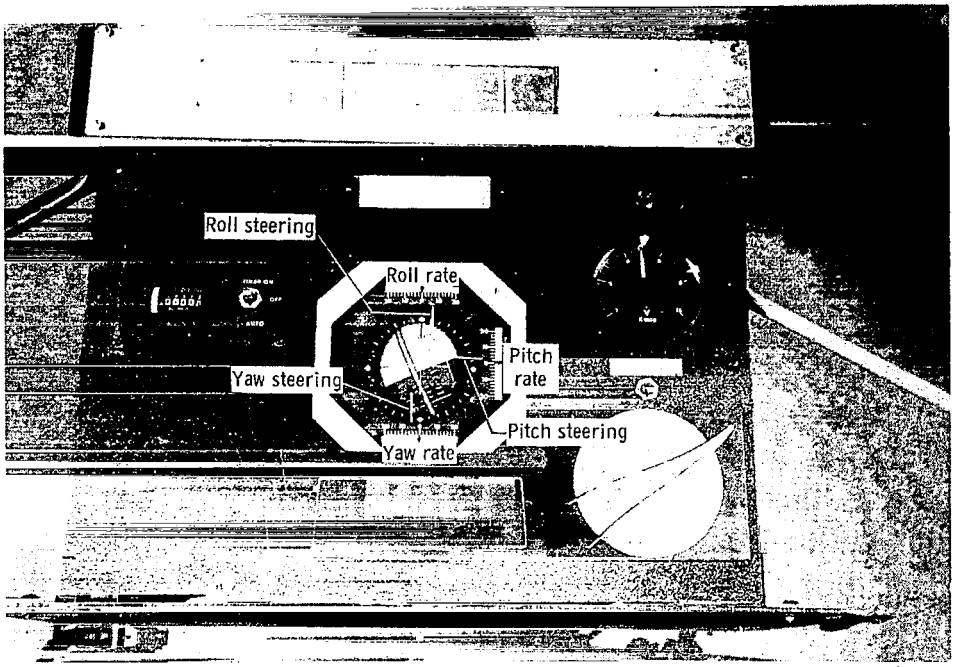

L-70-1347.1

Figure 10.- A pilot's view of the three-axis 8-ball in unmasked configuration.

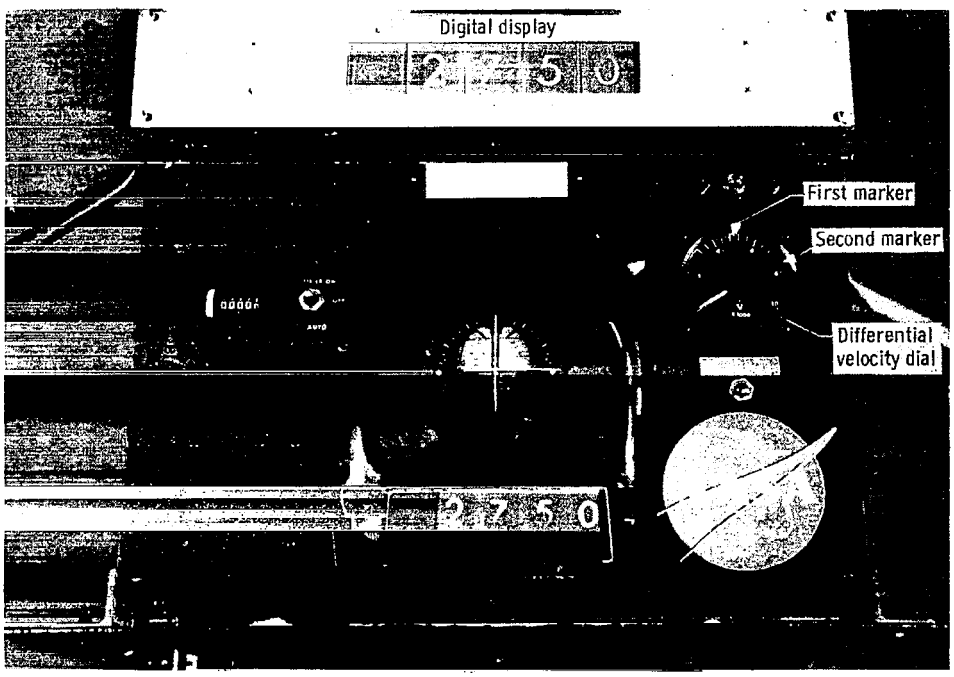

L-70-1350.1

Figure 11.- A pilot's view of the three-axis 8-ball with the attitude rate indicators masked.

LESS Computer Program

The analog-digital real-time computing system was selected for the LESS studies because a high degree of resolution was necessary in computing the LES ascent trajectories and resulting orbits. The LESS computer program was written for six-degree-of-freedom motion referenced to the center of the moon. The control-input loop of the program had provisions for selecting several modes of attitude control individually or in combination. In particular, the kinesthetic control input signals are active for all research runs, so the pilot and passenger must stand (or sit) relatively still when thrust-vector control or attitude jets are being used; this same feature, however, allows the pilot to use kinesthetic control inputs to augment either of the other two control modes.

The program was written in the FORTRAN IV computer language and had the option of selecting from four different numerical integration techniques. A sampling rate (and integration interval) of 1/32 of a second was used. This rate allowed sufficient accuracy for the trajectory calculations. Also, the digital outputs converted to smooth analog signals for driving the pilot's displays (i.e., the pilot saw 8-ball changes as continuous rather than stepped motions).

Other elements of the computer program such as equations, reference axes, and axis transformations are discussed in the appendixes. Appendix A contains a description of the reference axes and equations for generation of the various axis transformations in terms of direction cosines. Also, Euler angle expressions were extracted from appropriate elements of the transformation matrices; these expressions were then used to generate drive signals for the three-axis 8-ball. Appendix B contains derivations of the equations of motion in vector form and also in terms of body-axis components. The LESS inertia equations are constructed in appendix C, and finally equations for calculating pertinent LES orbital parameters are developed in appendix D.

Checkout of LESS Computer Program and Hardware

The LESS received two types of verification tests – the computer program only and then a full system test with a pilot and all the hardware tied in. By using the equations developed in the appendixes, the LESS computer program was test run in an analytical mode by means of a special automatic control loop.

To obtain initial conditions and other thrust and guidance parameter values for the test run, an independent digital computer program was written on the basis of the following planar-motion equations:

$$\left.\begin{aligned} \ddot{R}_O &= R_O\dot{\eta}^2 + \frac{F}{m}\cos\theta - \frac{\mu}{R_O^2} \\ R_O\ddot{\eta} &= \frac{F}{m}\sin\theta - 2\dot{R}_O\dot{\eta} \\ \dot{m} &= -\frac{F}{I_{sp}g_e} \end{aligned}\right\} \tag{1}$$

where I_{sp} is the specific impulse of the propellant and where the pitch angle θ is referenced to the local vertical. The pitch angle was constrained as follows:

$$\left.\begin{aligned} \ddot{\theta} &= \theta_1 = 0 && \left(0 \leqq t \leqq t_1\right) \\ \ddot{\theta} &= \frac{-1^o}{sec^2} && \left(t_1 < t < t_2\right) \\ \ddot{\theta} &= \frac{1^o}{sec^2} && \left(t_2 \leqq t \leqq t_3\right) \\ \left.\begin{aligned} \ddot{\theta} &= 0 \\ \theta_2 &= -90^o \end{aligned}\right\} && \left(t_3 < t \leqq t_{BO}\right) \end{aligned}\right\} \tag{2}$$

The 90^o pitch maneuver occurring between t_1 and t_3 takes approximately 19 seconds. Also, the thrust level F is changed from F_1 to F_2 at t_1 and remains at this second constant level until the time of burnout t_{BO}.

To obtain a set of trajectory burnout conditions which would place the LES in a 60-nautical-mile circular orbit, a series of iteration runs using equation sets (1) and (2) were made to determine values of F_1, F_2, t_1, and t_{BO}. For these runs an integration subroutine involving variable integration steps based on specified limits for computer round-off and truncation errors was used. Parameter values obtained from this iteration process (planar program values) are shown in table I. These planar program

TABLE I.- TRAJECTORY CHECKOUT PARAMETERS

Parameter	Values	
	Automatic LESS program	Planar program
(F_1/m) at $t = 0$, m/sec^2 (ft/sec^2) . . .	2.8032 (9.1968)	2.8103 (9.2201)
(F_2/m) at $t = t_1$, m/sec^2 (ft/sec^2) . . .	3.1504 (10.3360)	3.1503 (10.3356)
(F_2/m) at $t = t_{BO}$, m/sec (ft/sec^2) . .	5.4867 (18.0010)	5.4864 (18.0000)
t_1, sec	247.5	246.6
t_{BO}, sec	653.39	652.54

values were inserted in the LESS program (with the automatic-control loop), which was run several times with different numerical integration techniques and fixed-step integration intervals used. From these runs it was determined (1) that the automatic LESS program produced trajectory results in close agreement with those of the planar program, (2) that a fixed-step integration interval of 1/32 of a second was satisfactory, and (3) that the Runge-Kutta second-order (RKII) integration technique produced results almost identical to those obtained by using the more sophisticated fourth-order Runge-Kutta method. Thus, to reduce computation time, the RKII method with an integration interval of 1/32 of a second was selected for use in the piloted LESS program.

Before beginning the piloted LESS runs, the values in table I for the planar program were adjusted slightly to those shown for the automatic LESS program in order to obtain a more nearly circular reference orbit. The results of using both sets of values in their respective programs are shown in the tabular insert of figure 12. As indicated, neither solution produced an exactly circular orbit at a 60-nautical-mile altitude (60 n. mi. = 111 120 meters = 364 567 feet), but further iteration did not seem to be justified.

The results of a typical piloted LESS trajectory are shown in figure 12. Time histories of the piloted LESS trajectory state variables are shown on the left side of this figure, and the corresponding burnout conditions and orbital altitudes are given in the last column of the tabular insert. The top four traces on the left side give attitude histories; the fourth trace down gives the time history of the pitch angle before the 90° pitch maneuver (pitchover), and the trace directly above it gives the time history of the pitch angle after the 90° pitch maneuver. Both pitch and roll were controlled kinesthetically, and yaw was controlled by means of small on-off jets. It can be noted that both pitch-angle and roll-angle excursions increased with time into the flight; these increases occurred because the vehicle became more responsive and harder to control as it lost the majority of its mass (the propellant mass constituted over 60 percent of the initial mass).

Similar traces for the LESS operating with the automatic control loop are shown on the right side of figure 12. The roll and yaw angles were constrained to zero (not shown), and the pitch-angle history is shown on a single trace. Burnout conditions and orbital altitudes are given in the column of the tabular insert labeled "Automatic LESS;" these values were used as reference values for all the piloted LESS trajectories in which the automatic LESS guidance-parameter values listed in table I were used.

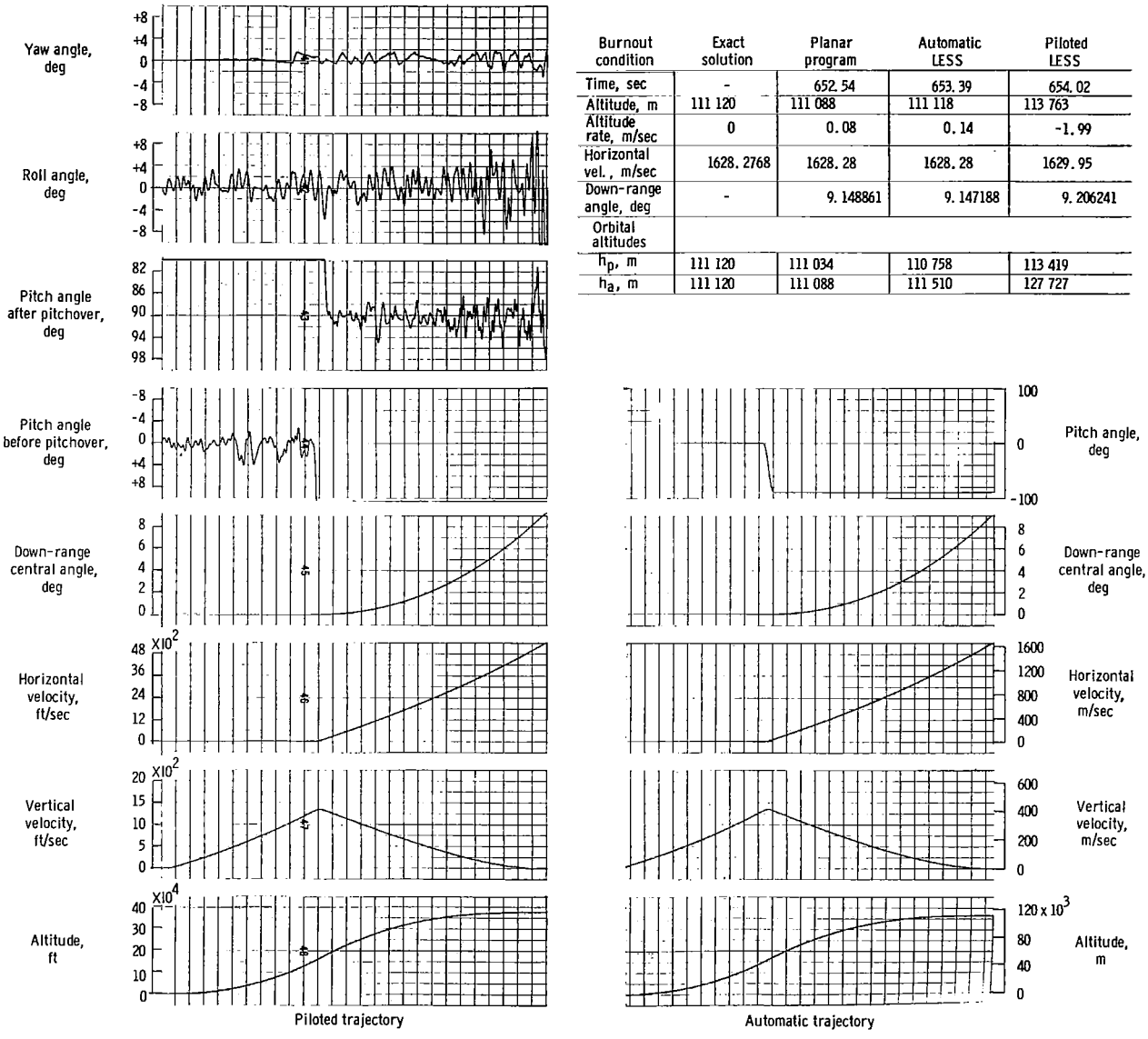

Burnout condition	Exact solution	Planar program	Automatic LESS	Piloted LESS
Time, sec	-	652.54	653.39	654.02
Altitude, m	111 120	111 088	111 118	113 763
Altitude rate, m/sec	0	0.08	0.14	-1.99
Horizontal vel., m/sec	1628.2768	1628.28	1628.28	1629.95
Down-range angle, deg	-	9.148861	9.147188	9.206241
Orbital altitudes				
h_p, m	111 120	111 034	110 758	113 419
h_a, m	111 120	111 088	111 510	127 727

Figure 12.- Illustrative time histories for a LESS automatic checkout trajectory and for a piloted trajectory in which the same guidance profile was used.

LESS EVALUATION

A pilot control station mounted on load cells for transmission of kinesthetic control inputs appeared to provide a valid simulation of a simplified lunar escape vehicle. During the checkout operations the test subjects were able to adapt to the equipment with a minimum of instruction and training. Alterations and additions to the control station hardware, to the attitude controller characteristics, and to the display instruments were made during the progress of the evaluation. The changes and reasons for making the changes are discussed in the following sections.

Test Environment

Several tests were made in which the pilot was in a pressure suit with a simulated portable life support system (PLSS). This configuration is illustrated in figure 13. The earth weight of the simulated PLSS, which is the load that a pilot might feel during a lunar escape lift-off, is approximately 311 newtons (70 lbf). For this photograph the pilot was posed to the left of his proper position in order to permit a view of the display panel from the available camera position.

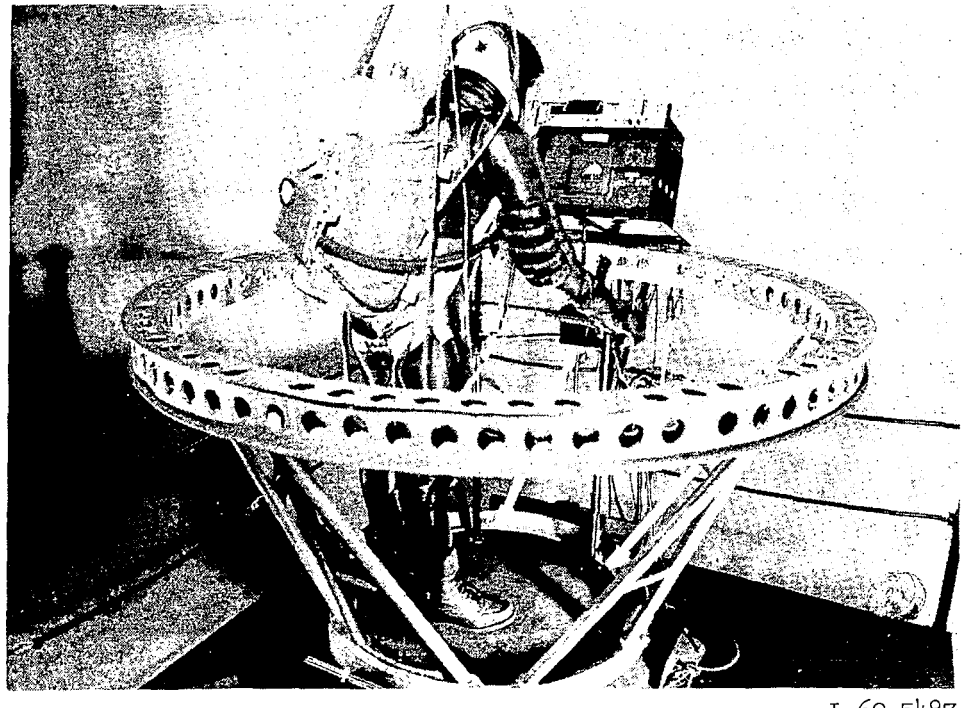

L-69-5487

Figure 13.- A view of the pilot during the tests which included a pressurized spacesuit.

Two hardware alterations were necessary in order to make the pilot control station compatible with pressure-suit operation. A handlebar, as shown in figure 8, was added to the handrail. The handlebar permitted the pilot to stand at the appropriate station c.g. position and maintain two-hand contact with the handrail. Also the thrust control switch could not be positively located by the pilot. The switch box was reoriented and the length of the switch lever was increased. The modified switch is the one shown in figure 8.

Controllers

The electrical dead band used in the axes of the three-axis controller appeared to affect control performance by the pilot when the controller was used as a simple on-off device. There was a degree of pilot uncertainty as to whether he had exceeded the dead band when he attempted to make a short-duration control input. The magnitude of the required control motion also caused an increase in the time required for the pilot to initiate a desired control input and sense the response. The controller dead-band effect was most detrimental when the pilot attempted a small yaw control input. Substitution of the single-axis yaw control stick was a definite improvement for the bang-bang type of yaw control input which was found to be preferred by the pilots when using kinesthetic control for pitch and roll during lift-offs. This control stick was particularly appropriate for the tests in which the pilot was in the pressure suit. The mechanism of the single-axis controller eliminated a requirement for control "feel" and permitted a more positive actuation of the stick-microswitch than was possible with the three-axis controller.

mation Display

Several alterations were made to the information display group. The final display group is shown in figure 11. The successful completion of a run was stressed rather than the fuel quantity used. Therefore the fuel-percentage indicator was eliminated. The fuel quantity was recorded, however, and can serve as design information.

As the tests continued, it became apparent that time was not always a valid situation clue to the pilot. If the vehicle had not accelerated to the proper velocity in the designated time, then the required orbit would not be achieved. The accumulated thrust-axis velocity was presented to the pilot by the large digital display at the top center of the panel. Several sizes of digital display numerals were tried before the test subjects were consistently able to read the displayed numbers without undue diversion of their attention from the 8-ball. The 2.29- by 1.52-cm (0.90- by 0.60-inch) size shown in figure 9 was satisfactory. The dial shown to the right provided a differential readout of

the velocity (with event markers). When the velocity approached that required for the pitch maneuver, the needle on the dial would begin to move. When the needle reached the first peripheral marker, the pilot would change the thrust and initiate the desired pitchover. The vernier needle was automatically reset at the end of its first traversal and did not move again until just prior to thrust-off. The second marker was used to indicate velocity for thrust-off. In most cases a single marker would be sufficient for all events. This differential readout enabled the pilots to execute the control events within 1 to 2 m/sec (3.3 to 6.6 ft/sec) of the scheduled velocity values. This range of error was a function of pilot reaction time, vehicle velocity, and vehicle thrust.

The test subjects tended to lose attitude orientation as they scanned the various items on the instrument panel. In particular a requirement to scan upward appeared to induce orientation problems. A mirror system was installed (see figs. 8 and 11) so that the subject could scan up or down to observe the digital display. All the test subjects considered the mirror system a very desirable addition to the panel.

The marking on the face of the 8-ball was the source of some difficulty during the tests. All of the escape profiles tested began with a pitch attitude of 0^{o} between the vehicle thrust axis (Z_B) and the local vertical. At this 8-ball position (see fig. 14(a)), the top half of the ball is white and the bottom half is black. The line of demarcation is, of course, the 0^{o} pitch mark. With the 8-ball at this position, the changes in pitch, roll, and yaw angles were readily interpreted and attitude orientation was easily maintained (compare figs. 14(a) and 14(b)). At a later point in the escape profiles, the desired pitch angle was in the vicinity of -90^{o}. At this angle the pilot's somewhat unfamiliar view of the 8-ball would appear as shown in figure 14(c). If oscillating changes in attitude occurred simultaneously in two or three axes, as shown in figure 14(d), the pilot could lose attitude orientation. In order to avoid this situation, a flip circuit was incorporated in the 8-ball reference circuit. As the pilot rotated in pitch from 0^{o} toward the -90^{o} attitude position, the 8-ball could be flipped some predetermined number of degrees so that the white-black portion of the 8-ball face could again be used for a reference. The flip circuit was activated as the vehicle pitch attitude passed through -60^{o} during the 90^{o} pitch maneuver. The change at this stage did not disturb the subject and was completed well before the pitch maneuver was to be terminated. The advantage gained by this procedure can be estimated by comparing figures 14(b) and 14(d). In a real situation, it would probably be more appropriate to mark the -90^{o} 8-ball pitch attitude position in a more acceptable fashion.

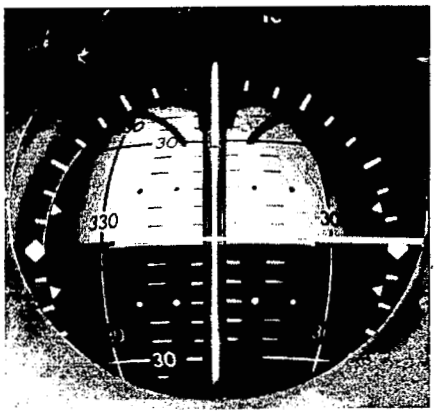

(a)

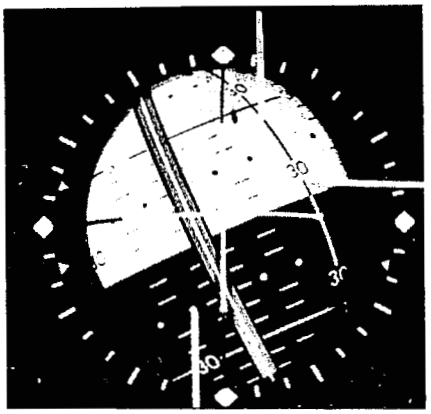

(b)

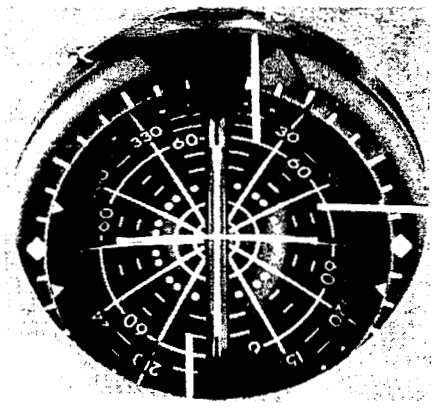

(c)

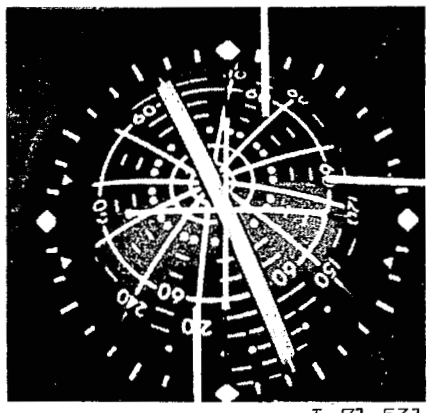

L-71-531

(d)

Figure 14.- The attitude reference display as seen by the pilot.

CONCLUDING REMARKS

A lunar-escape-system simulator was designed and fabricated to be used as a research tool to study problems related to lunar escape and simplified manual guidance and control. A pilot station mounted on load cells for transmission of kinesthetic control inputs to a digital computer program was shown to provide a valid simulation of a simplified lunar escape vehicle.

During checkout operations the test subjects were able to adapt to the equipment with a minimum of training and instruction.

Several hardware tradeoffs, primarily of the instrument display of situation information, made during the checkout resulted in an improved system concept applicable to the design of a prototype lunar escape vehicle. However, the physical size, arrangement, and complexity of the information display group were determined to be important factors affecting workload and attitude orientation for the lunar escape task.

Langley Research Center,
National Aeronautics and Space Administration,
Hampton, Va., February 19, 1970.

APPENDIX A

LESS AXIS SYSTEMS AND TRANSFORMATIONS

Body forces and moments acting on the LES are summed in a body-axis system (X_B,Y_B,Z_B) with origin at the vehicle instantaneous center of gravity (see fig. 15 in appendix B). Then for the trajectory and orbit calculations, velocity components are transformed to an inertial system (X_I,Y_I,Z_I) and to a local-vertical system (X_{LV},Y_{LV},Z_{LV}). The local-vertical system is used as a reference for a number of simplified LESS guidance and control schemes.

Transformation From Body to Inertial System

The body-axis components of the linear velocity of the LES (u,v,w) are transformed to inertial velocity components $(\dot{x}_I,\dot{y}_I,\dot{z}_I)$ by the matrix operation

$$\begin{bmatrix} \dot{x}_I \\ \dot{y}_I \\ \dot{z}_I \end{bmatrix} = \begin{bmatrix} a_{ij} \end{bmatrix} \begin{bmatrix} u \\ v \\ w \end{bmatrix} \qquad (i=1,2,3; \quad j=1,2,3) \tag{A1}$$

where the elements a_{ij} are direction cosines which were generated in the computer program (for the φ,ψ,θ order of Euler rotations) as follows from the body-axis angular velocity components (p,q,r):

$$\left.\begin{aligned} \dot{a}_{11} &= a_{12}r - a_{13}q & a_{31} &= a_{12}a_{23} - a_{22}a_{13} \\ \dot{a}_{21} &= a_{22}r - a_{23}q & a_{32} &= a_{21}a_{13} - a_{11}a_{23} \\ \dot{a}_{31} &= a_{13}p - a_{11}r & a_{33} &= a_{11}a_{22} - a_{21}a_{12} \\ \dot{a}_{22} &= a_{23}p - a_{21}r \\ \dot{a}_{13} &= a_{11}q - a_{12}p \\ \dot{a}_{23} &= a_{21}q - a_{22}p \end{aligned}\right\} \tag{A2}$$

Further discussion of this generation technique is given in reference 11. Then by referring to a standard matrix array of direction cosines (for the φ,ψ,θ order), the Euler angles can be extracted as

$$\left.\begin{aligned} \psi &= \sin^{-1}(a_{12}) \\ \theta &= \cos^{-1}\left(\frac{a_{11}}{\cos\psi}\right) \\ \varphi &= -\sin^{-1}\left(\frac{a_{32}}{\cos\psi}\right) \end{aligned}\right\} \tag{A3}$$

These expressions are used in the LESS program to drive an inertial attitude display (prototype LM 8-ball having a φ,ψ,θ gimbal order). Drive signals for an 8-ball which is slaved to the local vertical are discussed subsequently in this appendix.

Transformation From Inertial to Local-Vertical System

The inertial velocity components $\dot{x}_I$, $\dot{y}_I$, and $\dot{z}_I$ may be transformed to a rotating-local-vertical basis by

$$\begin{bmatrix} \dot{x}_{LV} \\ \dot{y}_{LV} \\ \dot{z}_{LV} \end{bmatrix} = \begin{bmatrix} c_{ij} \end{bmatrix} \begin{bmatrix} \dot{x}_I \\ \dot{y}_I \\ \dot{z}_I \end{bmatrix} \tag{A4}$$

where the elements c_{ij} are direction cosines generated as follows by using the angular velocities $\dot{\eta}$ and $\dot{\beta}$:

$$\left.\begin{aligned} \dot{c}_{11} &= -c_{31}\dot{\eta} & c_{13} &= c_{21}c_{32} - c_{22}c_{31} \\ \dot{c}_{12} &= -c_{32}\dot{\eta} & c_{23} &= c_{12}c_{31} - c_{11}c_{32} \\ \dot{c}_{21} &= c_{31}\dot{\beta} & c_{33} &= c_{11}c_{22} - c_{12}c_{21} \\ \dot{c}_{22} &= c_{32}\dot{\beta} \\ \dot{c}_{31} &= c_{11}\dot{\eta} - c_{21}\dot{\beta} \\ \dot{c}_{32} &= c_{12}\dot{\eta} - c_{22}\dot{\beta} \end{aligned}\right\} \tag{A5}$$

The angles η and β are described as the down-range and out-of-plane angles, respectively, and are defined by

$$\eta = \tan^{-1}\left(\frac{R_{x_I}}{R_{z_I}}\right) \tag{A6}$$

$$\beta = \tan^{-1}\left(\frac{R_{y_I}}{R_{z_I}}\right) \tag{A7}$$

where R_{x_I}, R_{y_I}, and R_{z_I} are inertial components of the position vector $\overline{R}_O$ discussed in appendix B.

Transformation From Body to Local-Vertical System

By using the preceding two transformations, the body-axis velocities u, v, and w can be transformed directly to the local-vertical system by

$$\begin{bmatrix} \dot{x}_{LV} \\ \dot{y}_{LV} \\ \dot{z}_{LV} \end{bmatrix} = \begin{bmatrix} c_{ij} \end{bmatrix} \begin{bmatrix} a_{ij} \end{bmatrix} \begin{bmatrix} u \\ v \\ w \end{bmatrix} = \begin{bmatrix} b_{ij} \end{bmatrix} \begin{bmatrix} u \\ v \\ w \end{bmatrix} \tag{A8}$$

where the direction-cosine elements b_{ij} have the typical form

$$b_{11} = c_{11}a_{11} + c_{12}a_{21} + c_{13}a_{31} \tag{A9}$$

It is not a simple matter to extract the Euler angles from the b_{ij} elements, so the following method is used. The components of local-vertical rotational rate can be expressed in the inertial system as

$$\begin{bmatrix} \omega_{LV,x_I} \\ \omega_{LV,y_I} \\ \omega_{LV,z_I} \end{bmatrix} = \begin{bmatrix} c_{ij} \end{bmatrix}^{-1} \begin{bmatrix} \dot{\beta} \\ \dot{\eta} \\ 0 \end{bmatrix} \tag{A10}$$

where $[\ ]^{-1}$ indicates a matrix inverse. Similarly, the body rotational rates can be referred to the inertial system by

$$\begin{bmatrix} \omega_{B,x_I} \\ \omega_{B,y_I} \\ \omega_{B,z_I} \end{bmatrix} = \begin{bmatrix} a_{ij} \end{bmatrix} \begin{bmatrix} p \\ q \\ r \end{bmatrix} \tag{A11}$$

After summing the two sets of rotational rates in the inertial system, the combined rotational rates may be referred back to the rotating-local-vertical system by

$$\begin{bmatrix} \omega_{x_{LV}} \\ \omega_{y_{LV}} \\ \omega_{z_{LV}} \end{bmatrix} = \left[a_{ij}\right]^{-1} \left\{ \left[a_{ij}\right] \begin{bmatrix} p \\ q \\ r \end{bmatrix} - \left[c_{ij}\right]^{-1} \begin{bmatrix} \dot{\beta} \\ \dot{\eta} \\ 0 \end{bmatrix} \right\} \tag{A12}$$

which reduces to

$$\begin{bmatrix} \omega_{x_{LV}} \\ \omega_{y_{LV}} \\ \omega_{z_{LV}} \end{bmatrix} = \begin{bmatrix} p \\ q \\ r \end{bmatrix} - \left[b_{ij}\right]^{-1} \begin{bmatrix} \dot{\beta} \\ \dot{\eta} \\ 0 \end{bmatrix} \tag{A13}$$

By using these rotational rates, Euler angle rates (indicating body rotational rates with respect to the local vertical for the φ,ψ,θ order) can be constructed as

$$\begin{bmatrix} \dot{\theta}' \\ \dot{\psi}' \\ \dot{\varphi}' \end{bmatrix} = \begin{bmatrix} \dfrac{\omega_{y_{LV}} \cos \varphi' - \omega_{z_{LV}} \sin \varphi'}{\cos \psi'} \\ \omega_{y_{LV}} \sin \varphi' + \omega_{z_{LV}} \cos \varphi' \\ \omega_{x_{LV}} - \dot{\theta}' \sin \psi' \end{bmatrix} \tag{A14}$$

These expressions can then be integrated to obtain Euler angles which relate the body rotations to the local-vertical system. The integrated expressions are used to generate drive signals for an 8-ball which is slaved to the local vertical.

APPENDIX B

DEVELOPMENT OF LESS MOTION EQUATIONS

This section deals with the formulation of motion equations for a body whose mass, moments of inertia, and center of gravity vary with time. These variations can occur when the propellant mass is a large percentage of the total mass of the body and the rate of propellant usage is high. Except for these mass changes, it is assumed that the body is essentially rigid.

Derivation of Force Equations

The force equations are obtained from the special case of the momentum theorem (see ref. 12), which states that the sum of all external forces on a rocket mass is equal to the sum of the time rate of change of the total linear momentum and the rate at which the exhaust-gas particles are transferring momentum out of the rocket system; that is,

$$\sum \overline{F}_{ext} = \frac{d}{dt}(m\bar{v}) - \dot{m}(\bar{v} + \bar{v}_e) \tag{B1}$$

where $\bar{v}$ is the velocity of the rocket mass m and where $\bar{v}_e$ is the exhaust velocity of the gas particles with respect to the mass m. After performing the indicated operations, this expression reduces to

$$\sum \overline{F}_{ext} = m\dot{\bar{v}} - \dot{m}\bar{v}_e \tag{B2}$$

In the lunar environment the significant forces acting on a rocket are thrust and the gravity. To separate these two forces and determine an expression for the thrust of the rocket, the test setup described in the following paragraph is considered.

A single rocket is held motionless in a test stand such that the thrust axis of the rocket is horizontal. During a firing test, $\dot{\bar{v}} = 0$, and the external forces are those due to gravity, the pressure at the exit nozzle of the rocket main thruster, and the restraint of the test stand. Equation (B2) then becomes

$$\overline{R}_O\left(\frac{\mu}{R_O^3}\right)m + \bar{p}_e A_e + \overline{F}_R + \dot{m}\bar{v}_e = 0 \tag{B3}$$

where the first term represents the gravity force, $\bar{p}_e$ is the directional pressure acting normal to the cross-sectional area of the exit nozzle (A_e), and $\overline{F}_R$ is the total restraining force of the test stand.

Next, only the horizontal components of the vectors which make up equation (B3) are considered – namely,

$$p_e A_e + \dot{m} v_e = -F_h \tag{B4}$$

where F_h is the horizontal component of $\overline{F}_R$. The rocket thrust $\overline{F}$ is equal and opposite to $\overline{F}_h$, and thus the terms on the left in equation (B4) represent the magnitude of the rocket-engine force (or gage thrust). Because $\bar{p}_e$ and $\bar{v}_e$ are always parallel to $\overline{F}$ in any orientation, equation (B2) can now be written as

$$\overline{F} + \overline{R}_O\left(\frac{\mu}{R_O^3}\right)m = m\dot{\bar{v}} \tag{B5}$$

where $\overline{R}_O$ acts toward the center of the moon; $\overline{F}$ is defined further in the next section.

Force Equations Expressed in Body-Axis System

The origin of the body-axis system (point O) is assumed at the instantaneous c.g. of the LES (see fig. 15). The initial c.g. location is designated point G and used for a point of reference. The following vector relations are used to define the LES forces in the body-axis system (components shown in brackets):

$$\bar{v}_G = \left[u', v', w'\right] \tag{B6a}$$

$$\bar{r}_{GO} = \left[\Delta x, \Delta y, \Delta z\right] \tag{B6b}$$

$$\overline{\omega} = \left[p, q, r\right] \tag{B6c}$$

$$\overline{\omega} \times \bar{r}_{GO} = \left[q\,\Delta z - r\,\Delta y,\ r\,\Delta x - p\,\Delta z,\ p\,\Delta y - q\,\Delta x\right] \tag{B6d}$$

$$\left(\frac{d}{dt}\bar{r}_{GO}\right)_{Body} = \left[\Delta\dot{x}, \Delta\dot{y}, \Delta\dot{z}\right] \tag{B6e}$$

$$\bar{v}_{GO} = \left(\frac{d}{dt}\bar{r}_{GO}\right)_{Body} + \left(\overline{\omega} \times \bar{r}_{GO}\right) \tag{B6f}$$

$$\bar{v}_O = \bar{v}_G + \bar{v}_{GO} \tag{B6g}$$

In equations (B6), $\bar{v}_O$ and $\bar{v}_G$ are the total linear velocities of point O and point G, respectively, with respect to the center of the moon, and $\overline{\omega}$ is the total rotational rate of the vehicle about point O; the subscript Body indicates that the differentiation in equation (B6e) is performed with respect to the body-axis system. The time derivative of $\bar{v}_O$ is obtained and substituted for $\dot{\bar{v}}$ in equation (B5); the resulting vector equation

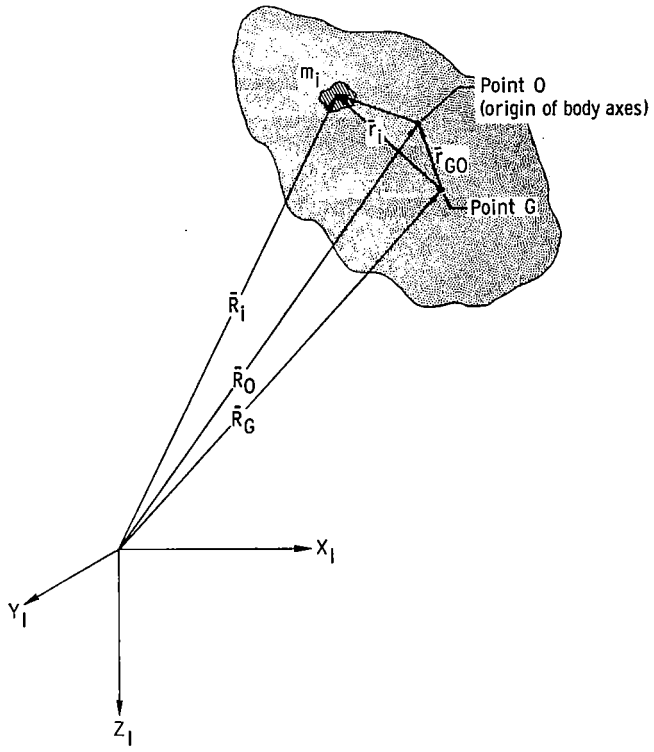

Figure 15.- LES position vectors with respect to points O and G and the center of the moon.

is then resolved into the following body-axis components to give simplified expressions for the body forces measured at point G:

$$\begin{bmatrix} F^*_{x_B} \\ F^*_{y_B} \\ F^*_{z_B} \end{bmatrix} = m \begin{bmatrix} \dot{u}' + w'q - v'r - \Delta x\left(q^2 + r^2\right) + \Delta y(pq - \dot{r}) + \Delta z(pr + \dot{q}) \\ \dot{v}' + u'r - w'p - \Delta y\left(r^2 + p^2\right) + \Delta z(rq - \dot{p}) + \Delta x(pq + \dot{r}) \\ \dot{w}' + v'p - u'q - \Delta z\left(p^2 + q^2\right) + \Delta x(rp - \dot{q}) + \Delta y(rq + \dot{p}) \end{bmatrix} \tag{B7}$$

The components $F^*_{x_B}$, $F^*_{y_B}$, and $F^*_{z_B}$ are thus body-axis components of the vector $\bar{F}^*$ (which is a combination of the thrust and the gravity forces). Equation (B7) is simplified in that all terms containing time derivatives of Δx, Δy, and Δz have been omitted as insignificant for the LESS study.

To relate $F^*_{x_B}$, $F^*_{y_B}$, and $F^*_{z_B}$ to measures at point O (origin of body-axis coordinates), the following relations are used:

$$\bar{v}_O = [u,v,w] \tag{B8a}$$

$$\dot{u} = u' + q\,\Delta z - r\,\Delta y \tag{B8b}$$

$$v = v' + r\,\Delta x - p\,\Delta z \tag{B8c}$$

$$w = w' + p\,\Delta y - q\,\Delta x \tag{B8d}$$

The u, v, and w expressions are solved for u', v', and w', respectively, and also differentiated. The resulting expressions are substituted into equation (B7) as indicated to obtain the following familiar equation

$$\begin{bmatrix} F^*_{x_B} \\ F^*_{y_B} \\ F^*_{z_B} \end{bmatrix} = m \begin{bmatrix} \dot{u} + wq - vr \\ \dot{v} + ur - wp \\ \dot{w} + vp - uq \end{bmatrix} \tag{B9}$$

The left side of equation (B9) can be expressed as

$$\begin{bmatrix} F^*_{x_B} \\ F^*_{y_B} \\ F^*_{z_B} \end{bmatrix} = \begin{bmatrix} F_{x_B} + b_{13}\left(\frac{\mu}{R_O^2}\right)m \\ F_{y_B} + b_{23}\left(\frac{\mu}{R_O^2}\right)m \\ F_{z_B} + b_{33}\left(\frac{\mu}{R_O^2}\right)m \end{bmatrix} \tag{B10}$$

where F_{x_B}, F_{y_B}, and F_{z_B} are the body-axis components of the main thrust $\bar{F}$ and the direction-cosine elements b_{13}, b_{23}, and b_{33} resolve the gravity force into the body-axis system. No additional thrust terms to represent attitude jets are included here because it is assumed that the jets will always be operated to produce force couples and thus any asymmetry due to the c.g. shift is discounted.

The main thrust $\bar{F}$ is further defined by

$$\begin{bmatrix} F_{x_B} \\ F_{y_B} \\ F_{z_B} \end{bmatrix} = \begin{bmatrix} F\xi_{x_B} \\ F\xi_{y_B} \\ -F \end{bmatrix} \tag{B11}$$

where F is the gage thrust and ξ_{x_B} and ξ_{y_B} are thrust misalinement angles (see fig. 16). Note that small-angle approximations have been assumed in equation (B11) because ξ_{x_B} and ξ_{y_B} are not expected to exceed $\pm 5^o$ even when the main thruster is gimbaled for control purposes. In the LESS studies ξ_{x_B} and ξ_{y_B} are generated either as a pilot's controller input (when using a gimbaled thruster) or as a fixed error (when using a fixed thruster).

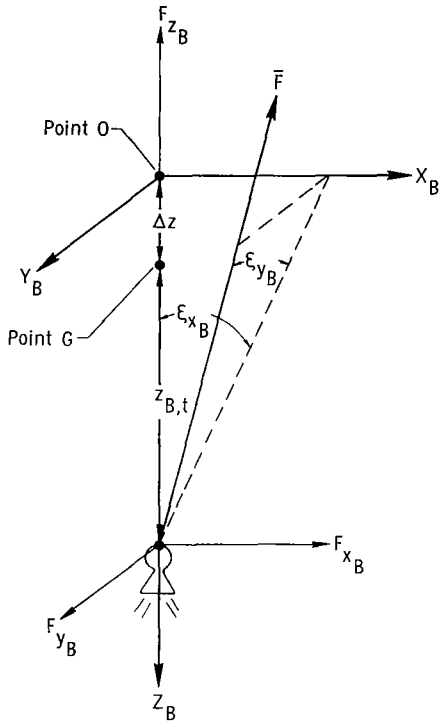

Figure 16.- Sketch showing LES thrust geometry.

Velocity-Along-the-Thrust-Axis Equation

During initial LESS studies it was assumed that a simple integrating accelerometer would be fixed at point G on the LES to measure only the accumulated velocity in the direction of thrust. The following equation was used in the LESS computer program to approximate this velocity reading:

$$V_{z_B} = \int_0^{t_{BO}} \left(\frac{F}{m} - b_{33} g_m - \Delta z \left(p^2 + q^2 \right) \right) dt \qquad \text{(B12)}$$

Moment Equations

The moment equations are written for body-axis coordinates whose origin is at the instantaneous c.g. of the LES (point O). The angular momentum about point O can be expressed (see fig. 15) as

$$\overline{N}_O = \sum_{i=1}^{\infty} \left[\left(\overline{R}_i - \overline{R}_O \right) \times m_i \left(\dot{\overline{R}}_i - \dot{\overline{R}}_O \right) \right] \tag{B13}$$

where the vectors $\left(\overline{R}_i - \overline{R}_O \right)$ can also be expressed as $\left(\bar{r}_i - \bar{r}_{GO} \right)$ with respect to the fixed body point (G). These vectors have the following components in the body-axis system (components shown in brackets):

$$\overline{R}_O = \left[R_{x_B}, R_{y_B}, R_{z_B} \right] \tag{B14a}$$

$$\bar{r}_i = \left[x_i, y_i, z_i \right] \qquad (i=1,2,\ldots,\infty) \tag{B14b}$$

$$\bar{r}_{GO} = \left[\Delta x, \Delta y, \Delta z \right] \tag{B14c}$$

$$\overline{R}_i - \overline{R}_O = \bar{r}_i - \bar{r}_{GO} = \left[x_i - \Delta x, y_i - \Delta y, z_i - \Delta z \right] \tag{B14d}$$

$$\dot{\overline{R}}_i - \dot{\overline{R}}_O = \begin{bmatrix} \left(\dot{x}_i - \Delta \dot{x} \right) + q \left(z_i - \Delta z \right) - r \left(y_i - \Delta y \right) \\ \left(\dot{y}_i - \Delta \dot{y} \right) + r \left(x_i - \Delta x \right) - p \left(z_i - \Delta z \right) \\ \left(\dot{z}_i - \Delta \dot{z} \right) + p \left(y_i - \Delta y \right) - q \left(x_i - \Delta x \right) \end{bmatrix} \tag{B14e}$$

With pilot movements disregarded, the LES is considered a rigid body, so $\dot{x}_i$, $\dot{y}_i$, and $\dot{z}_i$ are zero. Also, $\Delta \dot{x}$, $\Delta \dot{y}$, and $\Delta \dot{z}$ are assumed zero (see force equations), but Δx, Δy, and Δz must be retained in the moment equations for control purposes. With these assumptions, body-axis components of the angular momentum about point O can be expressed (after some algebraic manipulations) as

$$N_{x_B} = \sum_{i=1}^{\infty} m_i \left[\left(y_i - \Delta y \right)^2 + \left(z_i - \Delta z \right)^2 \right] p$$

$$- \sum_{i=1}^{\infty} m_i \left(z_i - \Delta z \right) \left(x_i - \Delta x \right) r - \sum_{i=1}^{\infty} m_i \left(y_i - \Delta y \right) \left(x_i - \Delta x \right) q \tag{B15a}$$

$$N_{y_B} = \sum_{i=1}^{\infty} m_i\left[(z_i - \Delta z)^2 + (x_i - \Delta x)^2\right]q$$

$$- \sum_{i=1}^{\infty} m_i(z_i - \Delta z)(y_i - \Delta y)r - \sum_{i=1}^{\infty} m_i(x_i - \Delta x)(y_i - \Delta y)p \qquad \text{(B15b)}$$

$$N_{z_B} = \sum_{i=1}^{\infty} m_i\left[(x_i - \Delta x)^2 + (y_1 - \Delta y)^2\right]r$$

$$- \sum_{i=1}^{\infty} m_i(y_i - \Delta y)(z_i - \Delta z)q - \sum_{i=1}^{\infty} m_i(x_i - \Delta x)(z_i - \Delta z)p \qquad \text{(B15c)}$$

By substituting appropriate inertia symbols for the various summation terms and assuming that the LES mass will be distributed symmetrically with respect to the X_BZ_B-, and Y_BZ_B-planes, the momentum components are reduced to

$$\begin{bmatrix} N_{x_B} \\ N_{y_B} \\ N_{z_B} \end{bmatrix} = \begin{bmatrix} I_{xx}p - I_{xz}r \\ I_{yy}q \\ I_{zz}r - I_{xz}p \end{bmatrix} \qquad \text{(B16)}$$

The following body-torque equations are obtained from the time derivatives of equation (B16):

$$\begin{bmatrix} Q_{x_B} \\ Q_{y_B} \\ Q_{z_B} \end{bmatrix} = \begin{bmatrix} I_{xx}\dot{p} + \dot{I}_{xx}p - I_{xz}(pq + \dot{r}) + (I_{zz} - I_{yy})rq \\ I_{yy}\dot{q} + \dot{I}_{yy}q + I_{xz}(p^2 - r^2) + (I_{xx} - I_{zz})rp \\ I_{zz}\dot{r} + \dot{I}_{zz}r + I_{xz}(rq - \dot{p}) + (I_{yy} - I_{xx})pq \end{bmatrix} \qquad \text{(B17)}$$

Terms containing $\dot{I}_{xz}$ are assumed negligible and thus omitted from equation (B17). The pitching acceleration $\dot{q}$ can be obtained directly from equation (B17) as

$$\dot{q} = \frac{Q_{y_B} - D_2}{I_{yy}} \qquad \text{(B18)}$$

where

$$D_2 = \dot{I}_{yy}q + I_{xz}(p^2 - r^2) + (I_{xx} - I_{zz})rp \qquad \text{(B19)}$$

The components Q_{x_B} and Q_{z_B} of equation (B17) can be solved simultaneously to yield

$$\dot{p} = \frac{I_{xz}\left(Q_{z_B} - D_3\right)}{I_{xx}I_{zz} - \left(I_{xz}\right)^2} + \frac{I_{zz}\left(Q_{x_B} - D_1\right)}{I_{xx}I_{zz} - \left(I_{xz}\right)^2} \tag{B20}$$

and

$$\dot{r} = \frac{I_{xz}\left(Q_{x_B} - D_1\right)}{I_{xx}I_{zz} - \left(I_{xz}\right)^2} + \frac{I_{xx}\left(Q_{z_B} - D_3\right)}{I_{xx}I_{zz} - \left(I_{xz}\right)^2} \tag{B21}$$

where

$$D_1 = \dot{I}_{xx}p + \left(I_{zz} - I_{yy}\right)qr - I_{xz}pq \tag{B22}$$

and where

$$D_3 = \dot{I}_{zz}r + \left(I_{yy} - I_{xx}\right)pq + I_{xz}qr \tag{B23}$$

For the LES studies Q_{x_B}, Q_{y_B}, and Q_{z_B} are defined as

$$Q_{x_B} = F\,\Delta y - F\xi_{y_B}\left(z_{B,t} - \Delta z\right) + Q_{J,x_B} + Q_{P,x_B} \tag{B24}$$

$$Q_{y_B} = F\xi_{x_B}\left(z_{B,t} - \Delta z\right) - F\,\Delta x + Q_{J,y_B} + Q_{P,y_B} \tag{B25}$$

and

$$Q_{z_B} = Q_{J,z_B} \tag{B26}$$

where $F\,\Delta x$ and $F\,\Delta y$ are kinesthetic control torques, Q_{J,x_B}, Q_{J,y_B}, and Q_{J,z_B} are attitude-jet torques, Q_{P,x_B} and Q_{P,y_B} are miscellaneous torques (e.g., torques due to uneven propellant drain), and $F\xi_{x_B}\left(z_{B,t} - \Delta z\right)$ and $F\xi_{y_B}\left(z_{B,t} - \Delta z\right)$ are thruster-misalinement-torque terms. The angles ξ_{x_B} and ξ_{y_B} can be either misalinement angles for a fixed main thruster or gimbal-travel angles for a gimbaled main thruster. The distance $z_{B,t}$ is the distance the main thruster is displaced (along the Z_B-axis) from the initial c.g. location (point G in fig. 16).

APPENDIX C

LESS INERTIA EQUATIONS

The LES vehicle moments and products of inertia are calculated with respect to the body-axis system (X_B, Y_B, Z_B) with origin at the instantaneous c.g. Because propellants comprise over one-half the system mass, there is considerable change of inertia during an escape-to-orbit run. Thus, inertia-rate effects need to be included in the LES moment equations.

Mass and Center-of-Gravity Relationships

For convenience the LES mass is divided into the following five parts: mass of basic vehicle (m_1), mass of passenger (m_2), mass of control pilot (m_3), combined mass of four spherical propellant tanks when empty (m_4), and mass of propellant in the tanks (m_5). Masses m_1, m_2, m_3, and m_4 are themselves constant, but the inertias associated with them are variable because the LES c.g. shifts significantly during an escape run. For clarity, the expression "LES c.g." is used herein to refer to the sum of the individual-mass c.g.'s (or the instantaneous total c.g.).

Body-axis coordinates of the following set of five position vectors $\bar{\rho}_{m_j}$ indicate the c.g. locations of the five individual masses with respect to the instantaneous c.g. of the LES:

$$\bar{\rho}_{m_1} = \left[\Delta x,\ \Delta y,\ \left(z_{G,1} - \Delta z\right)\right] \tag{C1a}$$

$$\bar{\rho}_{m_2} = \left[\left(x_{G,2} - \Delta x\right),\ \Delta y,\ \left(z_{G,2} - \Delta z\right)\right] \tag{C1b}$$

$$\bar{\rho}_{m_3} = \left[\left(-x_{G,2} + \delta x_{B,3} - \Delta x\right),\ \left(\delta y_{B,3}\right),\ \left(z_{G,2} - \Delta z\right)\right] \tag{C1c}$$

$$\bar{\rho}_{m_4} = \left[\left(x_{G,4} - \Delta x\right),\ \left(y_{G,4} - \Delta y\right),\ \left(z_{G,4} - \Delta z\right)\right] \tag{C1d}$$

$$\bar{\rho}_{m_5} = \left[\left(x_{G,4} - \Delta x\right),\ \left(y_{G,4} - \Delta y\right),\ \left(z_{G,4} - \delta z_{B,5} - \Delta z\right)\right] \tag{C1e}$$

The constants $x_{G,2}$, $y_{G,4}$, $z_{G,4}$, and so forth, are the coordinates of the various individual masses (identified by numeral in subscripts) with respect to the initial location of the LES c.g., and Δx, Δt, and Δz represent components of the LES c.g. shift during flight. The terms $\left(\delta x_{B,3} - \Delta x\right)$ and $\left(\delta y_{B,3} - \Delta y\right)$ represent the effective horizontal c.g. shift of the control pilot; $\delta x_{B,3}$ and $\delta y_{B,3}$ are the components of the actual movement of his c.g. from its initial location. The term $\delta z_{B,5}$ indicates how far the c.g. of the

propellant mass m_5 shifts downward as propellant is drained from the tanks. It is noted that $x_{G,4}$ and $y_{G,4}$ appear both in equation (C1d) and in equation (C1e); the reason is that the initial c.g. locations of m_4 and m_5 are coincident. Also, $x_{G,2}$ and $z_{G,2}$ appear both in equation (C1b) and in equation (C1c) because of the symmetrical location of the two masses m_2 and m_3.

Figure 17 is a partial illustration of the mass (and c.g.) relationships; X_G,Y_G,Z_G is a reference system (with origin at the LES initial c.g.) parallel to the primary X_B,Y_B,Z_B system. Typical mass locations are shown along with just the position vector to m_3 (mass of control pilot, including his suit and PLSS). For this setup, the control pilot (facing in x_B-direction) has moved forward $(\delta_{x_B,3})$ and to the right $(\delta_{y_B,3})$; this movement has effected a corresponding shift Δx and Δy in the total LES c.g. Also, the burnoff of propellants has caused the propellant c.g. to drop the distance $\delta_{z_B,5}$ from the m_4 position (i.e., initial m_5 position) to the m_5 position shown; this drop has caused the upward Δz shift in the total c.g. Thus, a change in the vector $\bar{\rho}_{m_3}$ can be caused both by propellant burnoff and the movements of the pilot himself (during kinesthetic control runs).

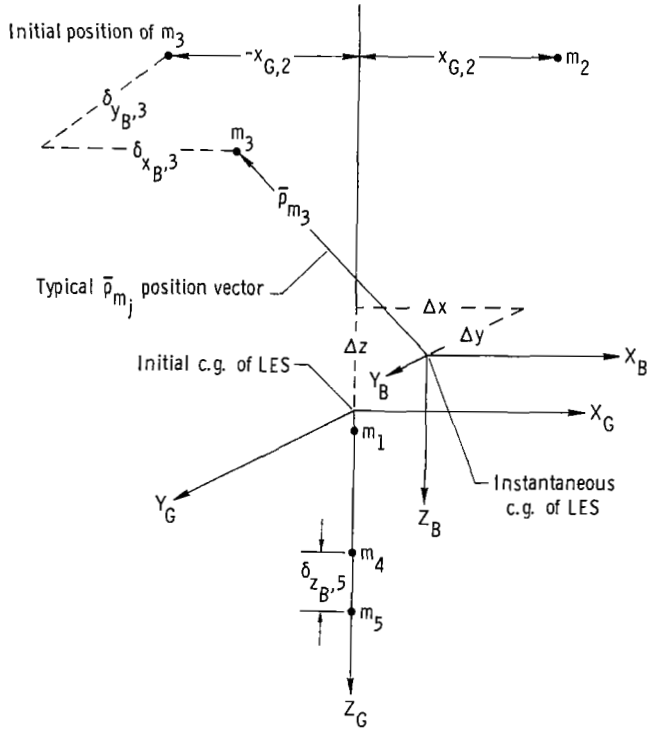

Figure 17.- LES mass and c.g. relationships.

Inertia Equations

The general forms of the inertia equations are given by

$$I_{xx} = \sum_{j=1}^{5}\left(I'_{xx_j} + m_j\rho^2_{x_j}\right) \tag{C2a}$$

$$I_{yy} = \sum_{j=1}^{5}\left(I'_{yy_j} + m_j\rho^2_{y_j}\right) \tag{C2b}$$

$$I_{zz} = \sum_{j=1}^{5}\left(I'_{zz_y} + m_j\rho^2_{z_j}\right) \tag{C2c}$$

and

$$I_{xz} = \sum_{j=1}^{5}\left(I'_{xz_j} + m_j\rho_{x_j}\rho_{z_j}\right) \tag{C2d}$$

In these equations the primes indicate inertias about individual reference axes X, Y, and Z (through each c.g.) which are parallel to X_B, Y_B, Z_B. Calculation of these "prime" inertias is straightforward except possibly for those associated with m_5, which are treated in the following section. Because of symmetry assumptions, I_{xy} and I_{yz} are zero.

Determination of Propellant Inertias

The "prime" inertias associated with the variable propellant mass m_5 (with respect to a reference system X,Y,Z through the center of a sphere) are herein constructed by a technique of summing elemental disks stacked in the z-direction (see fig. 18). Based on this figure, the following relationships can be written:

$$dV = \pi x^2 dz \tag{C3}$$

$$dm = \sigma\, dV \tag{C4}$$

$$x^2 = r_s^2 - z^2 \tag{C5}$$

$$\left(dI_{xx}\right)_{disk} = \frac{1}{4}x^2 dm \tag{C6}$$

where dV is the elemental disk volume, σ is the propellant mass density, and r_s is the radius of the sphere. The distance x is the radius of any particular disk; the value

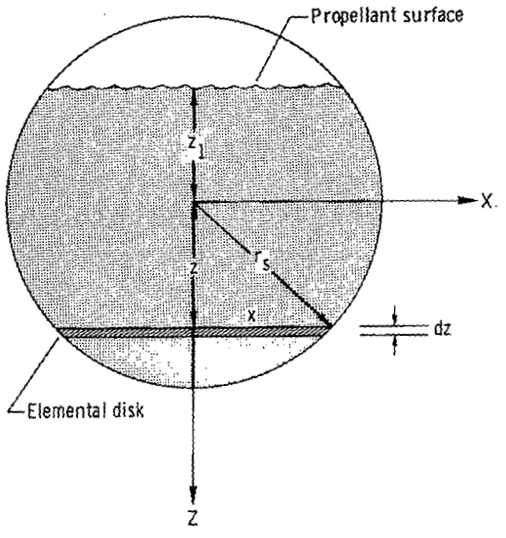

Figure 18.- Propellant-tank geometry showing typical elemental disk.

of x is determined by z, the distance of the disk from the center of the sphere. The distance z_1 is the vertical distance from the center of sphere to the top disk (viz., the propellant (top) surface). (The value of z_1 is negative when the propellant tank is more than one-half full.) The differential moment of inertia of an elemental disk with respect to temporary axis X through the center of the sphere is given by

$$dI'_{xx_5} = \left(dI_{xx}\right)_{disk} + z^2 dm \tag{C7}$$

The sum of all the disk-inertia differentials is then given by

$$I'_{xx_5} = \frac{1}{4}\int x^2 dm + \int z^2 dm$$

$$= \frac{\pi\sigma}{4}\int_{r_s}^{z_1}\left(r_s^2 - z^2\right)dz + \pi\sigma\int_{r_s}^{z_1} z^2\left(r_s^2 - z^2\right)dz \tag{C8}$$

For convenience, let σ be defined as the initial propellant mass (denoted $m_{5,o}$) divided by the volume of the sphere. By making this substitution and performing the indicated integrations, equation (C8) becomes

$$I'_{xx_5} = m_{5,o}\left(\frac{1}{5}r_s^2 - \frac{3}{16}r_s z_1 - \frac{1}{8}\frac{z_1^3}{r_s} + \frac{9}{80}\frac{z_1^5}{r_s^3}\right) \tag{C9}$$

When the propellant tanks are full, $z_1 = -r_s$ and the equation reduces to the familiar expression

$$I'_{xx_5} = m_{5,o}\left(\frac{2}{5} r_s^2\right) \tag{C10}$$

Similarly, when $z_1 = 0$ (tanks one-half full), the equation becomes

$$I'_{xx_5} = m_{5,o}\left(\frac{1}{5} r_s^2\right) = \frac{2}{5} m_5 r_s^2 \tag{C11}$$

where m_5 is here equal to one-half of the initial mass $m_{5,o}$.

By symmetry $I'_{xx_5} = I'_{yy_5}$, but I'_{zz_5} does not involve a transfer term for the elemental masses. However, I'_{zz} is similarly obtained by beginning with the relation

$$dI'_{zz_5} = (dI_{zz})_{disk} = \frac{1}{2}\left(r_s^2 - z^2\right)dm \tag{C12}$$

After all necessary operations have been performed, the result is

$$I'_{zz_5} = m_{5,o}\left(\frac{1}{5} r_s^2 - \frac{3}{8} r_s z_1 + \frac{1}{4}\frac{z_1^3}{r_s} - \frac{3}{40}\frac{z_1^5}{r_s^3}\right) \tag{C13}$$

APPENDIX D

CALCULATION OF ORBITAL PARAMETERS

The LESS computer program includes logic and equations for predicting the LES orbital characteristics based on the burnout conditions in the LES trajectory. In particular, the semimajor axis a is determined from

$$a = \frac{R_{O,BO}}{2 - \frac{R_{O,BO}(v_{O,BO})^2}{\mu}}$$

where the subscript BO denotes values of the state variables at burnout or orbit injection (i.e., when thrust is cut off). Next, the radius of pericynthion r_p can be determined from the following equation:

$$r_p = a\left[1 - \sqrt{1 - \frac{(R_{O,BO})^2(v_{O,h})^2_{BO}}{a\mu}}\right]$$

The altitude of pericynthion h_p is then given by

$$h_p = r_p - r_m$$

where r_m is the radius of the moon. The altitude of apocynthion h_a can now be calculated from the following expression:

$$h_a = 2a - r_p - r_m$$

The altitudes of pericynthion and apocynthion are the primary variables considered in determining whether the LES orbit is safe and/or satisfactory for rendezvous. The LESS computer program also contains equations for calculating orbital eccentricity, semilatus rectum, the central angle between injection and pericynthion, and the out-of-plane angle (i.e., the central angle between the LES position and the plane of the CSM). The equations for these variables are not given herein because this report is not primarily concerned with data.

REFERENCES

1. Economou, N.; et al.: A Study of Personnel Propulsion Devices for Use in the Vicinity of the Moon. Vol. I. NASA CR-365, 1966.

2. Economou, N.; et\al.: A Study of Personnel Propulsion Devices for Use in the Vicinity of the Moon. Vol. II. NASA CR-366, 1966.

3. Matzenauer, J. O.: Lunar Escape Systems (LESS) Feasibility Study. Vol. I – Summary Report. NASA CR-1619, 1970. Vol. II – Final Technical Report. NASA CR-1620, 1970.

4. Anon.: Study of One-Man Lunar Flying Vehicle. Vols. 1 to 6. SD-69-419-1 to SD-69-419-6 (Contract NAS 9-9045), North Amer. Rockwell Corp., Aug. 31, 1969. (Available as NASA CR-101917 to NASA CR-101923.)

5. Bergeron, Hugh P.; Adams, James J.; and Hurt, George J., Jr.: Analysis of Human Response in Combined Control Tasks. NASA TN D-4356, 1968.

6. Parlett, Lysle P.: Hovering Flight Investigation of Two Methods of Controlling a Man-Carrying Ducted-Fan Vehicle of the Flying-Platform Type. NASA TN D-841, 1961.

7. Hill, Paul R.; and Kennedy, T. L.: Flight Tests of a Man Standing on a Platform Supported by a Teetering Rotor. NACA RM L54B12a, 1954.

8. Zimmerman, C. H.; Hill, Paul R.; and Kennedy, T. L.: Preliminary Experimental Investigation of the Flight of a Person Supported by a Jet Thrust Device Attached to His Feet. NACA RM L52D10, 1953.

9. White, Ellis: Eastern Simulation Council Meeting. Simulation, vol. 12, no. 2, Feb. 1969, pp. 53-56.

10. Anon.: Apollo Operations Handbook – Lunar Module. Vol. I – Subsystems Data. LMA790-3-LM5 and Subsequent (NAS 9-1100), Grumman Aircraft Eng. Corp., Dec. 15, 1968. (Available from NASA.)

11. Rogers, A. E.; and Connolly, T. W.: Analog Computation in Engineering Design. McGraw-Hill Book Co., Inc., 1960.

12. Sutton, George P.: Rocket Propulsion Elements. Second ed., John Wiley & Sons, Inc., c.1956.

NASA-Langley, 1971 — 11 L-7364

04U 001 36 51 3DS 71088 00903
AIR FORCE WEAPONS LABORATORY /WLOL/
KIRTLAND AFB, NEW MEXICO 87117

ATT E. LOU BOWMAN, CHIEF, TECH. LIBRARY

"The aeronautical and space activities of the United States shall be conducted so as to contribute . . . to the expansion of human knowledge of phenomena in the atmosphere and space. The Administration shall provide for the widest practicable and appropriate dissemination of information concerning its activities and the results thereof."

—NATIONAL AERONAUTICS AND SPACE ACT OF 1958

NASA SCIENTIFIC AND TECHNICAL PUBLICATIONS

TECHNICAL REPORTS: Scientific and technical information considered important, complete, and a lasting contribution to existing knowledge.

TECHNICAL NOTES: Information less broad in scope but nevertheless of importance as a contribution to existing knowledge.

TECHNICAL MEMORANDUMS: Information receiving limited distribution because of preliminary data, security classification, or other reasons.

CONTRACTOR REPORTS: Scientific and technical information generated under a NASA contract or grant and considered an important contribution to existing knowledge.

TECHNICAL TRANSLATIONS: Information published in a foreign language considered to merit NASA distribution in English.

SPECIAL PUBLICATIONS: Information derived from or of value to NASA activities. Publications include conference proceedings, monographs, data compilations, handbooks, sourcebooks, and special bibliographies.

TECHNOLOGY UTILIZATION PUBLICATIONS: Information on technology used by NASA that may be of particular interest in commercial and other non-aerospace applications. Publications include Tech Briefs, Technology Utilization Reports and Technology Surveys.

Details on the availability of these publications may be obtained from:

SCIENTIFIC AND TECHNICAL INFORMATION OFFICE

NATIONAL AERONAUTICS AND SPACE ADMINISTRATION

Washington, D.C. 20546